Disentangling the chemistry and transport impacts of the Quasi-Biennial Oscillation on stratospheric ozone

Jinbo Xie[1#], Qi Tang[1], Michael Prather[2], Jadwiga Richter[3], Shixuan Zhang[4]

[1]Lawrence Livermore National Laboratory, Livermore, CA, USA

[2]Department of Earth System Science, University of California, Irvine, CA, USA

[3]National Center for Atmospheric Research, Boulder, CO, USA

[4]Pacific Northwest National Laboratory, Richmond, WA, USA

[#]now at Princeton University, New Jersey, NJ, USA

Correspondence to: Jinbo Xie (jinbo.xie@princeton.edu)

Abstract

The quasi-biennial oscillation (QBO) in tropical winds perturbs stratospheric ozone throughout much of the atmosphere via changes in transport of ozone and other trace gases and temperature changes, all of which alter ozone chemistry. Attributing these causes of the QBO-ozone variability may provide insight to model-to-model differences that contribute to ozone simulation. Here we develop a novel metric of steady-state ozone (SSO) to separate these effects: SSO calculates the local steady-state response of ozone due to the changes in temperature, chemical species, and overhead ozone column; the response due to circulation change is presumed when SSO shown no response. It is applied to the nudged Department of Energy's Energy Exascale Earth System Model version 2 (E3SMv2) with interactive ozone chemistry to demonstrate its validity. The E3SMv2 simulations nudged to reanalysis data produced reasonable wind and ozone patterns especially in the Tropics. Consistent with previous studies, we find clear demarcations with pressure. Ozone perturbations in the upper stratosphere (< 6 hPa) are predicted by the temperature changes; those between 6-hPa to 20-hPa are predicted by NO_y changes; and those in the lower stratosphere show no temperature or NO_y response and are presumably driven by circulation changes. These results are important for diagnosing model-to-model discrepancy in QBO-ozone response and enhancing reliability of ozone projections.

1. Introduction

The Quasi-Biennial Oscillation (QBO) is the principal mode of dynamical variability in the stratosphere. It is the key source of interannual variability in the overall chemical composition of the stratosphere (Randel et al., 1998; Shuckburgh et al. 2001; Park et al. 2017), manifest primarily through ozone (Reed 1964; Bowman, 1989; Wang et al., 2022).

The QBO affects ozone through both transport via atmospheric circulation and chemical processes via changed composition of the atmosphere (Reed, 1964; Holton et al., 1989; Gray and Dunkerton, 1990; Chipperfield and Gray, 1992; Chipperfield et al., 1994, Politowicz and Hitchman, 1997; Jones et al., 1998; Baldwin et al., 2001). The alternate change of QBO phase speeds up and slows down the vertical ascent in the tropics that pushes the ozone profile up and down; the QBO-temperature warms and cools the stratosphere that accelerates and decelerates ozone cycle; QBO-associated vertical transport of trace gas like reactive nitrogen reservoir NO_y may also affect ozone cycle.

Disentangling these causes of QBO-ozone variability is useful to understanding model-to-model discrepancy in the QBO-ozone simulation that contributes to improved ozone projections, such as the rate of ozone recovery that is still accompanied by large uncertainty due to internal climate variabilities like QBO (Chipperfield et al., 2017; Stone et al., 2018). Yet the role of chemical and dynamic process on QBO-ozone is still under debate (Zhang et al., 2021). Ling and London (1986) pointed to a close relationship between ozone and QBO-induced temperature anomaly and its associated photochemistry above 15-hPa. Chipperfield et al. (1994) and Tian et al. (2006) attribute the QBO-ozone to QBO modulation of NO_y species rather than the temperature changes above 10~15-hPa. Butchart et al., (2003), on the other hand, used a 3-D chemistry-climate model to argue that the transport is as important above 15~20-hPa. Currently, challenges in attributing QBO-ozone variability remain due to co-existent of chemistry and transport impact (Baldwin et al, 2001), and model limitations in simulating a free-running QBO variability (Richter et al., 2020) including asymmetry between QBO phases – a stronger and shorter QBO easterly phase and weaker and longer QBO westerly phase (Scaife et al., 2014; Richter et al., 2020). To separate the co-existent impacts, we built upon a novel use of the steady-state ozone (SSO) metric derived from the Linearized stratospheric ozone chemistry (Linoz; Mclinden et al., 2000; Hsu and Prather, 2009). The SSO assumes a "steady state" of ozone chemistry in stratosphere and is calculated in absence of dynamics, thereby isolates the

60   impacts due to chemical reactions and temperature perturbations. The determination of transport-

61   driven ozone is then based on the difference of modeled ozone from the steady-state ozone.

62   Studies have shown the validity of using linearized chemistry for representing ozone (Mclinden

63   et al., 2020) and ozone response to $4xCO_2$ (Meraner 2020), and our study build on it. The current

64   state-of-art earth system model still have problem in simulating a realistic QBO. Until now, only

65   15 of the 30 models in the Coupled Model Intercomparison Project phase 6 (CMIP6) have an

66   internally generated QBO (Richter et al., 2020). Within these models, the simulated QBO

67   amplitude and periods often fail to match the observed pattern. The World Climate Research

68   Project (WCRP) Atmospheric Processes And their Role in Climate (APARC) started an QBO

69   initiative (QBOi) in 2015 to improve Chemistry-Climate Model (CCM) simulation of tropical

70   variability (Butchart et al., 2018). The phase II of QBOi includes a set of nudging experiments to

71   examine QBO impact on climate, and here we build on those experiments.

72   In this study, we use the newly developed SSO metric on experiments following QBOi phase

73   II protocol to disentangle the chemical and transport impact of QBO on ozone. Our primary

74   modeling tool is the Department of Energy (DOE) Energy Exascale Earth Model version 2

75   (E3SMv2, Golaz et al., 2022) with interactive stratospheric ozone (Linoz v2 and Linoz v3;

76   McLinden et al., 2000; Hsu and Prather, 2009), and secondarily we examine some QBOi

77   experiments from the National Center for Atmospheric Research (NCAR) Community Earth

78   System Model (CESM). We also develop a new index of the QBO phase from a nonlinear

79   principal component analysis (NLPCA) of the tropical zonal winds that better retains asymmetric

80   patterns of QBO than standard linear PCA QBO index (Wallace et al., 1993). The phase-based

81   composite diagrams are then created to investigate the temporal evolution of ozone patterns, both

82   observed and modeled. We show that the SSO is a novel and effective tool in separating the

83   chemical and transport process of QBO on ozone, and may be applied to diagnose the model-to-

84   model discrepancy in QBO-ozone response. The observational data and ozone modeling are

85   described in Sect. 2. The NLPCA method is presented in Sect. 3, followed by the description of

86   the SSO in Sect. 4. The results are in Sect. 5. The discussion and conclusion are in Sect. 6.

87   ## 2. Data and methods

88   ### 2.1 CCM models

89   The primary model for this study is E3SMv2. E3SM's atmospheric component (EAMv2) is

90   run here as a CCM with specified sea surface temperatures (SSTs) and has 72 vertical layers and

91   a horizontal resolution of about 100 km. Following Richter et al. (2010), EAMv2 employs

92   gravity wave (GW) parameterizations that include orographic GWs (McFarlane, 1987),

93   convective GWs (Beres et al., 2004), and GWs generated by frontal systems (Charron and

94   Manzini, 2002). Tunable parameters in the orographic and frontal GW parameterizations remain

95   the same as in EAMv1 (Xie et al., 2018; Rasch et al., 2019). The tunable parameters in

96   convective GWs were explored to produce a more realistic QBO in EAMv2 with a period around

97   27 months, much closer to observations (28 months) as compared to 16 months in EAMv1

98   (Richter et al., 2019). Nevertheless, the modeled QBO remains weak in amplitude. Stratospheric

99   ozone in E3SMv2 is calculated interactively through transport and the chemical Linoz module

100   (McLinden et al., 2000; Hsu and Prather, 2009) that was updated from the E3SM O3v1 to O3v2

101   module (Tang et al., 2021). Linoz v2 data tables are used to calculate the 24-hour-average ozone

102   tendency (i.e., net production minus loss) from an adopted climatological mean state for key

103   species (CH_4, H_2O, and NOy, Cly, Bry) and first-order Taylor series expansions of the local

104   ozone, temperature, and overhead ozone column (see Eq. (3) in Sect. 4.1). The data tables are

105   generated for each year assuming key chemical species and families (CH_4, H_2O, and NOy, Cly,

106   Bry) follow monthly zonal-mean climatologies that scale with the slowly varying changes in

107   tropospheric mean abundance of their source gases (e.g., N_2O, CFCs, halons, CH_4, tropopause

108   H_2O). The Linoz model produces a reasonable stratospheric ozone climatology, including

109   seasonal and interannual variability and the Antarctic ozone hole (Tang et al., 2021; Ruiz and

110   Prather, 2022). The tropospheric chemical package for E3SMv2 (chemUCI) was not used and

111   the lower boundary for Linoz was set to 30 ppb. Thus, none of the ozone column variability

112   arises from tropospheric ozone chemistry. E3SMv2 diagnostics on the tendency of tropospheric

113   ozone calculate a geographically resolved stratosphere-troposphere exchange (STE) flux of

114   ozone every time step (Hsu et al., 2005; Tang et al., 2013).

115   The secondary model for this study is CESM2 (Emmons et al., 2020), using a modified

116   version of the community atmosphere model (CAM) with 83 vertical levels (Randall et al., 2023;

117   Isla et al., 2024), which is run here as a CCM with specified sea surface temperatures (SSTs).

118   CAM uses the finite-volume dynamical core with a nominal 1° horizontal resolution and with

119   physics from the Whole Atmosphere Community Climate Model version 6 (WACCM6;

120   Gettleman et al. 2019). The parameters for the convective GW momentum transport scheme is

121   tuned especially for this version to obtain a realistic, naturally generated QBO (Randall et al.,

122 2023). The inline ozone calculation in CESM2 is replaced with a monthly mean 3D ozone

123 climatology specified from a previous WACCM simulation. This input ozone forcing is formed

124 by merging WACCM simulations for historical (1850-2014, 3 members) and future period

125 (2015-2100, 1 member). As the mean of free-running CCM simulations, this ozone input

126 climatology does not have any significant QBO-like variability, and thus it cannot trigger a QBO

127 in the CCM (Butchart et al., 2023).

128   Both models are run with tropical winds being nudged to the observations and hence the

129 synchronicity of the QBO should be similar and we can compare directly with observations.

130 With the CESM2 QBO simulation we must limit our analysis to examining the forced dynamical

131 response (temperature, circulation), but with E3SM results we can to compare the modeled

132 QBO-ozone interactions with observations.

133   **2.2 Observed ozone and wind**

134   For ozone, we derive the observed QBO signal from the monthly zonal mean total column

135 ozone (TCO) using the Multi-Sensor Reanalysis version 2 data (MSRv2, R.J. van der A, et al.

136 2015). This latitude-by-month dataset initially covers the period 1979-2012 and later extended to

137 2020. For stratospheric profiles, we use the zonal monthly mean latitude-by-altitude from the

138 Concentration Monthly Zonal Mean (CMZM) product (Sofieva et al., 2023). This altitude-by-

139 month profile data covers the period 1985-2020. The vertical levels are converted to pressure

140 levels inverting the pressure-altitude formula, $z* = 16 \log_{10}(1000/P)$ km. We compared this

141 ozone data with the overlapping period from the Microwave Limb Sounder (MLS) data (V5

142 Level 3: Schwartz et al., 2021) and found only small differences with regard to QBO patterns.

143   We use ERA5 data (wind, temperature, geopotential height) from the reanalysis produced by

144 the European Center for Medium-Range Weather Forecast (ECMWF) Integrated Forecast

145 System (Hersbach et al., 2020). The version we use has 137 hybrid sigma model levels from the

146 surface to the model top at 0.01 hPa, and the horizontal resolution is about 31 km. We use

147 monthly mean data for the period 1979–2020 to analyze the QBO-related dynamical changes,

148 and 6-hourly ERA5 tropical zonal wind (15°N-15°S) to nudge model simulations mentioned

149 below. We use the 5°S-5°N tropical average zonal wind from ERA5 and simulations to

150 determinate the QBO phase index. The combined station zonal wind data from Freie University

151 of Berlin (Naujokat, 1986) for the period of 1979-2020 is also used.

152   **2.3 The QBOi simulations**

153   We use two experiments from the protocol for phase-2 of the QBOi (Butchart et al., 2018;

154   Bushell et al., 2020; Richter et al., 2020):

155   (1) Exp1-ObsQBO (nudged): the zonal wind in the tropical stratosphere is constrained to

156   follow the observed QBO evolution by nudging it toward ERA5 reanalysis (Hitchcock et

157   al. 2022). Thus, the stratospheric climate including temperature and circulation in the

158   tropics is constrained.

159   (2) Exp1-AMIP (natural): the zonal wind in the tropical stratosphere evolves freely in each

160   CCM being forced only by SSTs and trace-gas radiative forcing; there is no nudging.

161   The SSTs are historical and include interannual variability, primarily El-Nino and

162   Southern Oscillation (ENSO).

163   The nudging is applied to the zonal wind over the range 8 hPa-to-80 hPa and 15°S-to-15°N (Fig.

164   S1, nudging coefficient shown is for E3SMv2, that for CESM2 is similar). There is a slight

165   difference in how the models were nudged: E3SMv2 is nudged to the "full field" ERA5 wind

166   field including the longitudinal variability, while CESM2 is nudged to the zonally-averaged

167   ERA5 zonal wind field. The nudging relaxation timescale is 5 days. The current setup forces the

168   models to match the tropical QBO dynamic variability while allowing other variabilities to

169   evolve freely (e.g. semi-annual oscillation). For each experiment we produced 3 ensemble

170   members, and the ensemble mean is used for analysis.

171   To better understand the QBO-chemistry interactions, we performed two additional nudged

172   single-ensemble 1979-2020 runs with E3SMv2 using different chemical models: one with an

173   expanded stratospheric chemistry Linoz-v3 (Hsu and Prather, 2010), which calculates NO_y-N_2O-

174   CH_4-H_2O as prognostic tracers and includes their interactions with ozone; a second with fixed

175   ozone climatology as prescribed for CESM2.

3. NLPCA analysis of QBO phase

177   To build a time-line composite picture of the QBO in any variable, we need to define a phase

178   of each QBO and align these phases over a 28-month period. Phase asymmetry and nonlinear

179   features of the evolution of the QBO phase are found in many studies (Lindzen and Holton 1968;

180   Holton and Lindzen, 1972; Giorgetta et al., 2002). The most obvious and sharply defined

181   synchronization point is when the QBO west phase (QBOw, i.e. prevailing westerlies) transitions

182   to the east phase (QBOe: prevailing easterlies) at some pressure level in the middle stratosphere

183   (taken as 10 hPa here) (Naujokat et al., 1986; Pahlavan et al., 2021; Kang et al., 2022). The

184   QBOe phase is typically longer (e.g., Bushell et al., 2019) with wind speeds about twice as

185   strong as that of the QBOw (Naujokat et al., 1986; Kang et al., 2022). The problem with defining

186   the QBO phase (index) simply as the month-to-month difference relative to the synchronization

187   point (e.g., Ruiz et al., 2021) is that the duration of different phases varies across successive

188   QBOs.

189   Previous use of PCA-derived QBO indices (Wallace et al., 1993) did not allow for this

190   asymmetric and nonlinear behavior. Lu et al. (2009) noted that the reconstructed wind series

191   from the PCA looked more sinusoidal in time than the actual winds, and thus the asymmetries

192   between phases did not show up in the PCA-based indices. To address these issues, we use an

193   NLPCA method that utilizes hierarchical-type neural network with an auto-associative

194   architecture (Scholz et al. 2002). It is a nonlinear generalization of the standard PCA from

195   straight lines to curves in the original data space, and natural extension to the PCA method by

196   enforcing the nonlinear components to the same hierarchical order as in the standard PCA

197   (Scholz et al., 2002). The NLPCA model described here has 5 layers with 3 hidden layers of

198   neurons. The layers of the neural-network for NLPCA are in the sequence of input-encoding-

199   bottleneck-decoding-output with the structure of n-(2k+2)-k-(2k+2)-n, where the n refers to

200   dimension of input/output dataset and k is the number of dimensions for bottleneck layer. To

201   achieve robustness, the NLPCA is applied to the tropical zonal wind data (5°S-5°N, 10-hPa to

202   70-hPa) for a set of k varying from 2 to 5, with 100 runs (different in random initialization

203   weights) for each k. The optimal number of k is set as 5 as it gives the lowest root-mean-square-

204   error between the input and output. The comparison of QBO phase angles and QBO transition

205   points are shown in Fig. S2a and S2b. It is shown that the first and second principal components

206   (PC1 and PC2) of the NLPCA account for approximately 90% of the whole variance (Figs. S2c

207   and S2d).

208   Following previous studies (Wallace et al., 1993; Hamilton and Hsieh, 2002; Lu et al., 2009),

209   the QBO phase index ψ is calculated using PC1 and PC2 as follows:

210   $$\psi = arctan\,(v/u)   (-\pi \leq \psi \leq \pi),   (1)$$

211   where u and v are the time series of the PC1 and PC2, respectively. The positive/negative phase

212   angle index ψ corresponds to QBOw/QBOe.

213   We compare the reconstructed zonal wind anomalies using NLPCA and PCA (Wallace et al.,

214   1993) with the QBO cycle in the observation (Fig. 1). It is shown that the observed QBO

215   transition corresponds to an abrupt downward propagation in QBOw and a slower downward

216   transition in QBOe (indicated by clustering points in B to C to A on black triangular shape in

217   Fig. 1a). The NLPCA captures large part of this sharp transition in QBOw while PCA

218   underestimates it (indicated by points near C in Fig. 1a). This difference is also clearly shown in

219   a typical QBO cycle of 1970. September – 1972. March (Figs. 1b, 1c, and 1d, black arrow-sticks

220   exhibits the downward propagation in QBOw) and the time series of NLPCA/PCA QBO phase

221   (index) (Fig. S2).

222   NLPCA-derived QBO index is more realistic in following the atmospheric changes, it is

223   impractical to map the NLPCA phases onto the monthly-mean model diagnostics. Thus, our

224   QBO composites use simple monthly time steps about our best synchronization point, which

225   from the NLPCA analysis we take to be at the transition when phase angle index ψ crosses 0

226   with negative values before and positive values after it (from QBO easterly to QBO westerly

227   phase). It is demonstrated that comparing to QBO composites produced using the PCA-derived

228   QBO index, those that produced using the NLPCA-derived index show a shifted QBO

229   synchronization month (Fig. S2b). This results in larger contrast in observed tropical zonal wind

230   anomalies between QBOw/QBOe (Figs. S3a and S3b) that is consistent with those described in

231   previous literatures (Hamilton and Hsieh, 2002; Lu et al., 2009). This larger contrast between

232   NLPCA and PCA in zonal wind anomalies is correspondent with the larger contrast in that of the

233   total column ozone anomalies (Figs. S3c and S3d).

234   # 4. Linoz calculation of the steady-state ozone

235   To examine the chemical ozone response to the QBO we use the SSO calculated from both

236   Linoz v2 and v3 models. For Linoz-v2, this metric calculates local SSO response of ozone to the

237   modeled changes in temperature, chemical species, and overhead ozone column; for Linoz-v3,

238   more long-lived species are added. For Linoz v2 the SSO is derived from Eq. 4 of McLinden et

239   al. (2000). The photochemical SSO mole fraction f_{ss} (parts per million, moles per mole of dry air)

240   is expressed as follows:

241
$$f^{ss} = f^o + [\, (P-L)^o + \frac{\partial(P-L)}{\partial T}|^o \, (T-T^o) + \frac{\partial(P-L)}{\partial C_{O_3}}|^o (C_{O_3} - C_{O_3}^o) \,]\tau, \qquad (2)$$

242   This is derived by setting $\frac{d(P-L)}{dt} = 0$ for Eq. 1 in McLinden et al., (2000). The values f^o, T^o,

243   and $C_{O_3}^o$ are the climatological values of local ozone, temperature, and overhead column ozone

244   tables used to calculate the Linoz tendencies. *(P–L)ₒ* is the ozone net production minus loss

245 tendency and the partial derivatives are the sensitivity of the net production to temperature and
246 overhead column ozone.

247   A major assumption of Linoz v2 here is that the key chemical families (NO_y, Cl_y, Br_y) and
248 long-lived reactive gases (N_2O, CH_4, H_2O) do not change from their climatological values used
249 to generate the tables (Hsu and Prather, 2009). This steady-state calculation ignores transport
250 tendencies and thus will be apply only where the photochemistry is rapid, i.e., $\tau =$
251 $-[\frac{\partial (P-L)}{\partial f}|_o]^{-1} < 100$ days. Fig. 2 shows this Linoz v2 steady-state calculation (f_{SS}, T, τ) for
252 January and July using ERA5 monthly mean temperature.

253   An alternative version (Linoz v3) of the SSO derived from Hsu and Prather (2010) is
254 expressed as follows:

255 $$f_{ss} = f_o + [(P-L)_o + \frac{\partial (P-L)}{\partial T}|_o (T - T_o) + \frac{\partial (P-L)}{\partial C_{O_3}}|_o (C_{O_3} - C_{O_3}^o) + \sum_{j=1}^{j=5} \frac{\partial (P-L)}{\partial f_j}|_o (f_j - f_j^o)]\tau, \quad (3)$$

256 This is similar as Eq. 2, except adds the contribution from sources of f_{N2O}, f_{NOy}, f_{CH4}, f_{H2O}. This
257 may be used to provide a more precise diagnosis of the SSO from those models that have these
258 output of chemistry species in addition to the temperature profile.

259 5. Impact of QBO on circulation and stratospheric ozone

260   Nudging the tropical zonal wind creates QBO-driven perturbations to the temperature and
261 residual circulation that we can diagnose in both the E3SMv2 and CESM2 runs and compare
262 with observations. For E3SMv2 with interactive ozone we are able to see the changes in ozone.
263 This also applies to the simulations with an internally generated QBO.

264   We create a similar composite of the QBO cycle using E3SMv2/CESM2 following Ruiz et
265 al., (2021) to see the full QBO cycle influence on stratospheric ozone. The time-composite is
266 created for each month starting 14 months prior and extending to 14 months after the QBO
267 transition for 1979-2020. The center of the composite is when the NLPCA-derived QBO phase
268 angle index (see Sect. 3) shifts from negative to positive (QBOe -> QBOw). We create
269 composites for circulation (zonal wind, temperature and residual circulation) and chemistry
270 tracers (total column ozone (TCO), ozone concentration, NO_y) as a function of QBO phase. For
271 TCO, we calculate the zonal-mean averages to produce the global map of composite; for all other
272 fields, we process the tropical (15°S-15°N) and extratropical (30°S-60°S/30°N-60°N) vertical
273 profile of regional average using latitudinal weight to produce the composites. The CESM2
274 ozone composite is not shown since its ozone is prescribed.

275   The structure for this section is as follows: we first analyze the impact of nudged QBO on

276   circulation in E3SM and CESM in Sect. 5.1, we then analyze its impact on global TCO and

277   tropical/extratropical ozone in Sect. 5.2 and 5.3. The chemistry and transport impact of QBO are

278   further analyzed using the SSO metric in Sect. 5.4. The overall performances of the models are

279   summarized in Sect. 5.5.

280   **5.1 Impact of QBO on circulation**

281   In this section, we examine the impact of nudged QBO on circulation in both E3SMv2 and

282   CESM2. We first analyze its impact on zonal wind and subsequently on temperature and residual

283   circulation (e.g. $\underline{w}^*$, which characterizes the transport impact of the Brewer-Dobson Circulation).

284   Through nudging, the anomalous tropical zonal wind (15°S-15°N) in both nudged E3SMv2

285   and CESM2 simulations exhibit a similar negative-positive-negative pattern to that of ERA5

286   from QBOe to QBOw (Fig. 3). In terms of the magnitude, E3SMv2 zonal wind's pattern above

287   6-hPa is minorly stronger than that of ERA5 and CESM2. Despite this minor difference, both

288   models overall reproduce the QBO signal in the tropical nudging regions. Correspondent to the

289   zonal wind changes shown in Fig. 3, the tropical temperature (Figs. 4a-c) in both models exhibit

290   a negative-positive-negative-positive pattern like that of ERA5. Alongside is the residual vertical

291   transport $\underline{w}^*$ that exhibits a positive-negative-positive-negative pattern, like that of ERA5 (Figs.

292   4d-f). Studies have documented the QBOe tends to relate to cooling and upward advection while

293   QBOw relates to warming and downward advection (Baldwin et al., 2001). The tropical

294   temperature and $\underline{w}^*$ results shown are thus in-phase with zonal wind change in both models.

295   In the extratropic region (30°N-60°N/30°S-60°S), the results for the zonal wind are noisier

296   (Fig. S4). The ERA5 results exhibit scattered signals of zonal wind changes for both hemispheres

297   (Fig. S4a). The two models exhibit noisy results like that of ERA5, with CESM2 closer to ERA5.

298   This is expected since the extratropics are more likely to be affected by dynamic noise from the

299   polar regions. Unlike that of the zonal wind, the temperature and residual vertical transport $\underline{w}^*$

300   results are smoother for both observation and nudged simulations. It is shown that ERA5 exhibits

301   about two cycles of positive-negative phase change for temperature (Fig. 5a and 5d) and

302   negative-positive phase change for $\underline{w}^*$ (Figs. 6a and 6d) from QBOe to QBOw, although

303   southern hemisphere (SH) is noisier than northern hemisphere (NH). Both models seem to have

304   better agreement with ERA5 in the NH (Figs. 5b, 5c and Figs. 6b, 6c), while E3SMv2 performs

305   better than CESM2 in the SH (Figs. 5e, 5f and Figs. 6e, 6f). Studies have documented that the

306   QBO signal in the extratropical temperature and vertical advection are at about 180° phase

307   change relative to the tropical QBO signal (Baldwin et al., 2001). The results shown here are in-

308   phase with our nudged QBO signal in the tropics. Overall, the two models show some signals of

309   QBO-related signals outside of the regions of nudging on temperature and $\underline{w}^*$, exhibiting the

310   "spill-over" effect of QBO nudging.

311   To sum up, nudging creates a more realistic QBO signal in both E3SMv2 and CESM2

312   especially in the tropical region. Outside of the nudging region, the "spill-over" effect of the

313   nudged QBO is seen mostly on temperature and $\underline{w}^*$ but less on the noisier zonal wind.

5.2 Impact of QBO on global TCO

315   In this section, we examine the impact of QBO on ozone using TCO reanalysis (MSRv2) and

316   E3SMv2 model simulations. The TCO composites from the E3SMv2 nudged simulation is

317   compared in Fig. 7. It is shown that the anomalous MSRv2 TCO exhibits a significant shift of

318   tripole pattern from QBOe to QBOw (Fig. 7a). The MSRv2 exhibits tri-pole pattern of

319   anomalous low TCO in the tropics and high in the extratropics during QBOe that gradually

320   transits to tri-pole pattern of anomalous high in the tropics and low in the extratropic during

321   QBOw. The magnitude of the negative in QBOe (5 DU) is lower than the positive pattern (12

322   DU) in QBOw in the tropics, indicating asymmetric phase response of TCO to QBO in the

323   tropics. The E3SMv2 nudged simulation is like MSRv2 in that it captures most of the tripole

324   patterns in both phases with similar amplitudes (Fig. 7b), indicating the impact of nudged QBO

325   on TCO is close to what observed. It is shown that the internally generated QBO variability in

326   E3SMv2 natural (Fig. S5a) only partly exhibits the patterns of MSRv2 with weaker amplitude

327   (nearly eight times weaker). Since the response of column ozone is mainly driven by the wind in

328   the lower stratosphere, this discrepancy likely indicates that the internal generated QBO is too

329   weak there. This and the good result in nudging run (Fig. 7b) indicate that nudging the tropical

330   zonal wind contributes to the modulation and enhancement of this "QBO-driven" TCO

331   variability in E3SMv2.

332   Overall, the nudged E3SMv2 simulations show "QBO-driven" TCO variability in accordance

333   to observation that is partly present in E3SMv2 natural simulations and enhanced by QBO

334   nudging.

5.3 Impact of QBO on tropical/extratropical stratospheric ozone

336   In this section, we analyze the impact of QBO on tropical (15°S-15°N) and extratropical

337   (30°S-60°S/30°N-60°N) stratospheric ozone concentration. The composites of ozone vertical

338   profile (1-hpa to 100-hPa) from E3SMv2 nudged and E3SMv2 Linoz-v3 nudged simulations are

339   compared with the CMZM satellite data (Fig. 8).

340   In the tropics, it is shown that the CMZM satellite ozone exhibits a double-peak vertical

341   structure with large ozone variations between 1~20-hPa and 20~100-hPa (Fig. 8a). Both peaks

342   shift in a sequence of negative-positive-negative from QBOe to QBOw, and the amplitude of the

343   upper peak is smaller than that of the lower peak (Fig. 8a). The E3SMv2 nudged simulation

344   captures most of the double-peak structure (Fig. 8b) with minor exceptions – the anomalous high

345   ozone in CMZM from month -14 to month -8 around 10-hPa and the anomalous low around 10-

346   hPa from month -2 to month 2 is missed. Studies have documented NO_y variations as the

347   primary drivers of ozone QBO changes around this range (Chipperfield et al., 1994; Tian et al.,

348   2006). Since nudged E3SMv2 simulation uses the Linoz-v2 which the chemical species such as

349   CH_4 or NO_y remain constant, the deficiency may be due to uncertainty in these chemical species.

350   To test this assumption, we also compared the E3SMv2 Linoz-v3 nudged simulation (with

351   chemistry of NO_y-N_2O-CH_4-H_2O included) with CMZM (Fig. 8c). It is shown that the E3SMv2

352   Linoz-v3 nudged simulation captures both missing ozone fluctuation between 6-hPa to 10-hPa in

353   E3SMv2 nudged, indicating that this missing chemistry may be responsible for this deficiency.

354   The E3SMv2 natural simulations, on the other hand, show similar double-peaked patterns but

355   with smaller amplitude (3 times weaker) and shorter period (Fig. S5b). This may be because the

356   period of internally generated QBO in E3SMv2 is ~21 years (Golaz et al., 2022). Overall, the

357   E3SMv2 nudged simulation modifies the period and enhances the QBO response in tropical

358   ozone that is mostly consistent with the CMZM weaker above 20-hPa and stronger below 20-

359   hPa.

360   This analysis is extended to the E3SMv2 nudged simulations in the extratropical region in

361   both hemispheres (30°N-60°N/30°S-60°S). Since the nudging is imposed only in the tropical

362   regions, we can further examine the impact of nudged QBO in the extratropics where it is free

363   running. Fig. 9 shows pressure-time cross-section of the extratropical (30°N-60°N/30°S-60°S)

364   ozone concentration as a function of QBO phase for CMZM satellite ozone, E3SMv2 nudged

365   and E3SMv2 Linoz-v3 nudged simulations. Unlike that of the tropics, the extratropical ozone for

366   CMZM is noisier despite an overall in-phase change with QBO (Figs. 9a and 9d). The exception

367   is in the NH where the QBOw exhibits an extra phase change to positive (Fig. 9a). It is shown

368   that nudged E3SMv2 simulations follow the similar positive-negative ozone phase shift in both

369   hemispheres (Figs. 9b and 9e) without the noisy phase changes in the NH. In terms of the

370   amplitude, the QBOw is similar for both hemispheres but being weaker than CMZM in QBOe.

371   The ozone change in the E3SMv2 Linoz-v3 nudged simulation tends to be similar to that of the

372   E3SMv2 nudged simulation, except the amplitude in QBOw is stronger (Figs. 9c and 9f).

373   Overall, the E3SMv2 nudged and E3SMv2 Linoz-v3 nudged partly capture in-shift with QBO in

374   extratropical ozone in both hemispheres despite amplitude difference.

375   **5.4 Separating the chemistry and transport impact of QBO on ozone using**

376   **steady-state ozone**

377   In this section, we utilize the SSO (Eq. 2 and 3, see Sect. 4 for detail) introduced in Sect. 4

378   to separate the chemistry and transport impact of QBO on ozone. As a coupled system, the QBO

379   chemical and transport impacts on ozone are intertwined, making it difficult to diagnose which

380   QBO impact is more prominent to the ozone differences between model and observation or

381   among different models. Here we try to quantitatively separate these two terms with this new

382   diagnostic tool, recognizing their time scale differences. We first derive the Linoz-v2 SSO (Eq.

383   2) for E3SMv2 nudged and CESM2 nudged simulations (Fig. 10). Although ozone is prescribed

384   in CESM2, the SSO for CESM2 shown here is the temperature-ozone impact due to the CESM2

385   temperature profiles. To further analyze impact of temperature and different chemistry species

386   (NO_y, N_2O, H_2O, CH_4) in ozone simulation, the SSO using temperature only (Eq. 2) and using

387   temperature plus chemistry species (Eq. 3) are derived for E3SMv2 Linoz-v3 nudged (Fig. 11).

388   In the tropics (15°S-15°N), the Linoz-v2 SSO from E3SMv2 and CESM2 nudged exhibit an

389   apparent negative-positive-negative pattern above 20-hPa (Figs. 10a and 10d). These

390   corresponds to the temperature patterns above 20-hPa shown in the previous section (Figs. 4b

391   and 4c). This pattern in E3SMv2 is like that of the E3SMv2 ozone pattern above 20-hPa (Fig.

392   8b), indicating a temperature impact mostly above 20-hPa. Below 20-hPa, the prognostic ozone

393   in E3SMv2 correspond to the alternating $\underline{w}^*$ shift patterns (Fig. 4e). The residual meridional

394   circulation shows a weaker magnitude below 20-hPa and is thus less likely to play a major role

395   in ozone change (Fig. S6). This and the lack of response in SSO indicates the prognostic ozone

396   below 20-hPa in E3SMv2 is transport-driven. Like that of the analysis in the tropics, the

397   temperature impact in the extratropics (30°N-60°N/30°S-60°S) is stronger above 20-hPa for both

398   E3SMv2 (Figs. 10b and 10c) and CESM2 (Figs. 10e and 10f) nudged simulations. The

399   difference is that temperature in the SH (30°S-60°S) is overall noisier than that of the northern

400   hemisphere (30°N-60°N). This noisier SH SSO above 20-hPa in the nudged simulations

401   correspond to the noisier temperature for the two models (Figs. 5c and 5f), which may be largely

402   affected by stronger and noisier southern polar vortex (Fig. S7) as also documented by other

403   studies (Ribera et al., 2004). The intrusion of the polar vortex via event like sudden stratospheric

404   warming (Butler et al., 2017) may have an impact on the QBO-ozone relationship in the

405   extratropics. Below 20-hPa, the E3SMv2 nudged ozone corresponds to the $\underline{w}^{*}$ (Fig. 10b and

406   10e), indicating it's transport-driven. Overall, with the application of Linoz-v2 on E3SMv2

407   nudged simulation, we can partly separate the temperature-driven and transport-driven QBO-

408   ozone around the boundary of 20-hPa in both tropics and extratropics. The limit in this

409   application lies in the uncertainty in exclusion of chemistry transport such as NOy in the

410   simulations.

411   To test the sensitivity of the results to the chemistry variations, we further applied Linoz-v2

412   SSO (Eq. 2, temperature-only) and Linoz-v3 SSO (Eq. 3, temperature plus chemistry) to

413   E3SMv2 Linoz-v3 nudged simulation (Fig. 11). It is shown that the SSO including temperature

414   plus chemistry variation show better accordance with MSRv2 ozone (Figs. 8a, 9a, 9d) than

415   including temperature only especially in both the tropics (Figs. 11a, and 11d) and the extratropics

416   (Figs. 11c, 11d, 11e, and 11f). This better accordance is especially apparent between 6-hPa to 20-

417   hPa and in good accordance with the NO_y change (Fig. 12), indicating the impact of chemistry

418   variation within this height. To further examine the variable responsible for the change, we also

419   did the single specie sensitivity test (not shown). It is shown that including temperature plus NO_y

420   variation can reproduce the patterns in Figs. 11a-c. This indicates the NO_y variation an important

421   driver around 6-hPa to 20-hPa in QBO-ozone, in accordance with the previous studies

422   (Chipperfield et al., 1994; Tian et al., 2006).

423   The results here indicate demarcations of QBO-induced ozone at 6-hPa and 20-hPa. These

424   demarcations of the QBO-induced ozone at 6-hPa and 20-hPa may be due to the separation of

425   ozone lifetime below/above 20-hPa (Reed et al., 1964) and NO_y variation (Chipperfield et al.,

426   1994; Tian et al., 2006). The ozone lifetime is relatively long compared with the dynamical

427   process below 20-hPa while shortened considerably above it. The temperature affects ozone

428   above 20-hPa (especially above 6-hPa) through ozone destruction – warmer anomalies accelerate

429 ozone destruction, leading to correspondent ozone decrease (Wang et al., 2022), vice versa; the

430 transport effect of QBO-related wind modulates the temperature through thermal wind balance

431 enhancing/lessening the upward motion in the tropics (Plumb and Bell, 1982; Baldwin et al.,

432 2001; Ribera et al., 2004; Punge et al., 2009). In the extratropics, the process is similar except

433 that is controlled by the return branch of QBO-induced circulation that is in 180° phase reversal

434 with the tropics (Baldwin et al., 2001). This explains the apparent separation of transport- and

435 chemistry-driven ozone changes above/below 20-hPa. Between 6-hPa to 20-hPa, QBO

436 modulation of NO_y variation is shown to be an important contributor of the QBO-ozone cycle in

437 addition to the temperature impact (Chipperfield et al., 1994). This explains the better

438 reproduction of SSO above 20-hPa when including NO_y variation. Ozone transport, on the other

439 hand, plays a relatively weaker role above 20-hPa. Overall, the demarcations of QBO-induced

440 ozone shown here can be overall explained by photochemical process above 6-hPa, NO_y

441 variation between 6-hPa and 20-hPa, and circulation change in vertical advection below 20-hPa.

442 It is also worth mentioning that the nudged CESM2 also produces similar temperature and $\underline{w^*}$.

443 This indicates that nudged CESM2 may produce similar prognostic ozone if Linoz were to be

444 implemented as interactive ozone module.

5.5 Model performance in simulating QBO impact

446 In this sub-section, we examine the overall performance of E3SMv2 and CESM2 QBOi

447 simulations in simulating the QBO-ozone relationship. We evaluate the pattern correlation and

448 standard deviation of the area-weighted TCO pattern (60°S-60°N), vertically-weighted ozone

449 concentration (15°S-15°N, 30°N-60°N, 30°S-60°S), zonal wind (15°S-15°N, 30°N-60°N, 30°S-

450 60°S), temperature (15°S-15°N, 30°N-60°N, 30°S-60°S), and $\underline{w^*}$ (15°S-15°N, 30°N-60°N, 30°S-

451 60°S). For ozone, only E3SMv2 results are shown since CESM2 has fixed ozone. The results are

452 summarized in a Taylor diagram shown in Fig. 13. The observed pattern is plotted at the (1,0)

453 reference point.

454 In terms of ozone (Fig. 13a), there are remarkable differences between the simulations.

455 Overall, the E3SMSv2 nudged simulations perform the best, with the pattern correlation of all

456 four variables over 0.8 while other simulations are below 0.5. This indicates nudging realistic

457 QBO variability may increase the model performance in simulating ozone. In the extratropics,

458 the E3SMv2 nudged simulation has good pattern correlations, but the amplitude is off by over

459   1.5 times. The results for temperature, zonal wind and $\underline{w}^*$ are similar with ozone in the tropics

460   (Figs. 13b, 13c, and 13d). What's different is in the extratropics — both nudged

461   E3SMv2/CESM2 temperature, zonal wind, and $\underline{w}^*$ show better performance in NH extratropics

462   than in SH extratropics. This may be due to stronger polar vortices in SH and NH that disturb the

463   QBO signal (Ribera et al., 2004). Another difference is in the natural simulations – the tropical

464   temperature (15°S-15°N) and zonal wind signals exhibit reasonable correlations of over 0.7 in

465   zonal wind, over 0.5 in temperature. This indicates a discernable internally generated QBO

466   signal in the E3SMv2/CESM2, although it's weaker and does not extend to the extratropics.

467   # 6. Discussion and conclusion

468   ## 6.1 Discussion

469   There are some interesting issues worth discussing in this section. First, the use of the SSO

470   provides an useful tool to diagnose the dynamical and chemical impact of the QBO on ozone. The

471   Linoz v2 SSO metric can be applied to all models with the minimum need of temperature profile

472   only. One caveat of this approach is that Linoz-v2 SSO neglects the potential impact of cross-over

473   chemical species such as the NO_y as in SSO that has been shown to be an important driver for

474   QBO-ozone change between 6-hPa to 20-hPa. Thus, it would be recommended to include at least

475   the NO_y output by the CCMs and include it in SSO calculation (Eq. 3) for a more precise diagnostic

476   between this height range. The QUasi-Biennial oscillation and Ozone Chemistry interactions in

477   the Atmosphere (QUOCA) proposed a new joint QBOi-CCMI project to improve understanding

478   of the QBO-ozone feedback in present-day and future climates. The tools shown here may be

479   useful to diagnose the uncertainty in QBO-ozone relationship among different model simulations

480   in this project.

481   Another noteworthy issue is the nudging employed in the current study. Nudging has been

482   adopted by models from different climate centers in the QBOi project to ensure the realistic

483   simulation of QBO through constraining the tropical climate. The different strategies of nudging

484   in these models and their effects on the QBO climate are thus needed to be analyzed with care.

485   Our study showed that the nudging overall constrains both E3SMv2 and CESM2 towards a

486   realistic representation of QBO-associated temperature and residual circulation field outside of the

487   nudged regions (15°S-15°N tropics). However, differences in the nudging strategies can play a

488   role in the detailed features of the zonal wind and temperature simulated by the two models. For

489 example, the extratropical zonal wind and temperature in CESM2 showed more scattered features

490 than those in E3SMv2 in our simulations. This may be partly because the full field nudging in

491 E3SMv2 nudge all zonal wavenumbers. This may pose a stronger constraint on field than the zonal

492 mean nudging in CESM2 that may nudge less spectrum of zonal wavenumbers.

493 Thirdly, our study shows the importance of including NO_y-N_2O-CH_4-H_2O chemistry in the

494 linearized ozone representation of climate model. Our study shows that the E3SMv2 Linoz v2

495 simulation with linearized ozone may underestimate the QBO-ozone amplitude above 10-hPa, as

496 also documented in Meraner et al., (2020). The E3SMv2 Linoz-v3 simulation with NO_y-N_2O-CH_4-

497 H_2O chemistry, on the other hand, improves this QBO-ozone magnitude especially between 6-hPa

498 to 10-hPa. Meraner et al., (2020) demonstrated the usefulness of linearized ozone in representing

499 ozone due to negligible computational cost, despite its deficiency in simulating QBO-ozone

500 magnitude. The inclusion of NO_y-N_2O-CH_4-H_2O chemistry may contribute to alleviating this

501 issue.

502 Last, the impact of ozone feedback on the climate in this study deems further attention. The

503 two models compared here show overall similar QBO-signal over the nudging runs despite have

504 two different ozone modules – one interactive and another non-interactive. One may question what

505 the results would be with the same modules under nudging. The sensitivity test of E3SMv2 fixed-

506 ozone nudged simulation shows that with fixed-ozone, the temperature patterns are still retained

507 although with an amplified magnitude in both the tropics and extratropics (Fig. S8). This indicates

508 a strong nudging impact, and an overall damping effect of interactive ozone in E3SMv2.

509 6.2 Conclusion

510 In this study, we utilize the SSO on nudged climate model simulations to separate the chemical

511 and transport response of the QBO ozone impact. We derive a new QBO phase index using the

512 NLPCA method and utilize this index to form QBO cycle composites to analyze QBO-ozone

513 relationships in observation and simulations. By analyzing the simulations from two QBOi

514 participant models (E3SMv2 and CESM2), we found that the nudged simulations can produce a

515 reasonable QBO impact in the tropics and create "spill-over" impact to the extratropical fields like

516 temperature and residual circulation. The nudged E3SMv2 simulation captures the tripole

517 composite pattern in the observed TCO. Nudging was also shown to improve the double-peaked

518 vertical structure in observed ozone data between 1~20-hPa and 20~100-hPa over the tropics. In

519 the extratropics outside of the nudging region, the nudged E3SMv2 simulated ozone tends to be

520 overall in-phase with the observed but with magnitude difference, indicating the "spill-over"

521 impact of nudged QBO signal.

522 Utilizing the SSO metric, we separated the chemical and transport response of ozone in

523 E3SMv2 nudged to QBO. It is shown that these impacts have rather clear demarcations on both

524 tropical and extratropical ozone response at 6-hPa and 20-hPa – chemistry impact correspondent

525 to QBO-related temperature changes dominates the response above 6-hPa linked to photochemical

526 processes and between 6-hPa to 20-hPa linked to NO_y variation, and transport impact related to

527 QBO-related vertical advection dominates the response below 20-hPa. The results here are

528 important for diagnosing model-model and model-observation differences in the QBO with free-

529 running climate simulations, allowing us to separate chemical from circulation effects.

530 Stratospheric ozone is not only essential for protecting life on the Earth but also has

531 important climate impacts. More and more studies reported the important role of ozone

532 variations in modifying the stratospheric circulation and therefore influencing the surface climate

533 (e.g. Xie et al., 2020). Since the QBO has relatively high predictability, considering its impacts

534 on stratospheric ozone and subsequent atmospheric circulations may help improve the

535 predictions of surface weather and climate (e.g., Li et al., 2023).

536 Despite the above studies, however, there are still caveats. The current study makes use of

537 only one model in QBOi that has an interactive ozone feature. More models may be used in the

538 future to examine the QBO-ozone relationship. These are to be assessed in future studies.

539

Data availability

541 The satellite data from the Copernicus Climate Change Service can be accessed at

542 (https://cds.climate.copernicus.eu/cdsapp#!/dataset/satellite-ozone-v1?tab=form). The ERA5

543 data can be accessed at (https://cds.climate.copernicus.eu/cdsapp#!/dataset/reanalysis-era5-

544 complete?tab=overview). The ChemDyg diagnostics can be accessed at

545 (https://doi.org/10.5281/zenodo.11166488).

546

Author contribution

548 J.X., Q.T. designed the research; J.X. performed the E3SM simulations and wrote the

549 manuscript. J.R. provided the CESM2 simulation. Q. T. and M.P.'s supervised the research and

550 helped interpreting the results. All authors contributed to the scientific discussion and paper
551 revision.
552

Competing interests

554 The authors declare that they have no conflict of interest.
555

Acknowledgement

557 We thank the Copernicus Climate Change Service for providing the satellite data and ECMWF
558 for the ERA5 data. We thank Isla Simpson for setting up the CESM2 QBOi simulations, and
559 providing the Python script for generating the Transformed Eulerian Mean variables. We thank
560 Sasha Glenville for transferring the CESM2 data. This research was supported as part of the
561 E3SM project, funded by the U.S. Department of Energy, Office of Science, Office of Biological
562 and Environmental Research. Part of the work was supported by the LLNL LDRD project 22-
563 ERD-008 titled "Multiscale Wildfire Simulation Framework and Remote Sensing". E3SM
564 simulations were performed on a high-performance computing cluster provided by the BER
565 ESM program and operated by the Laboratory Computing Resource Center at Argonne National
566 Laboratory. Additional post-processing and data archiving of production simulations used
567 resources of the National Energy Research Scientific Computing Center (NERSC), a DOE
568 Office of Science User Facility supported by the Office of Science of the U.S. Department of
569 Energy under Contract No. DE-AC02-05CH11231. This work was performed under the auspices
570 of the U.S. Department of Energy by Lawrence Livermore National Laboratory under contract
571 DE-AC52-07NA27344. The IM release number is LLNL-JRNL-858987. This work was in part
572 supported by the National Center for Atmospheric Research (NCAR), which is a major facility
573 sponsored by the National Science Foundation (NSF) under Cooperative Agreement 1852977.
574 Portions of this study were supported by the Regional and Global Model Analysis (RGMA)
575 component of the Earth and Environmental System Modeling Program of the U.S. Department of
576 Energy's Office of Biological and Environmental Research (BER) via NSF Interagency
577 Agreement 1844590.

Reference

Andrews, M. B., Knight, J. R., Scaife, A. A., et al.: Observed and Simulated Teleconnections Between the Stratospheric Quasi-Biennial Oscillation and Northern Hemisphere Winter Atmospheric Circulation, J. Geophys. Res., 124, 1219–1232, https://doi.org/10.1029/2018JD029368, 2019.

Andrews, D.G., J.R. Holton, and C.B. Leovy: Middle Atmosphere Dynamics. Academic Press, 489pp, 1987.

Anstey, J. A. and Shepherd, T. G.: High-latitude influence of the quasi-biennial oscillation, Q. J. Roy. Meteor. Soc., 140, 1–21, https://doi.org/10.1002/qj.2132, 2014.

Baldwin, M. P., Birner, T., Brasseur, G., et al.: 100 years of progress in understanding the stratosphere and mesosphere, Meteor. Mon.,59, 27.1–27.62, https://doi.org/10.1175/AMSMONOGRAPHSD-19-0003.1, 2019.

Baldwin, M. P., Gray, L. J., Dunkerton, T. J., et al., The quasi-biennial oscillation, Rev. Geophys., 39, 179–229, 2001.

Baldwin M. P., Tung KK., Extra-tropical QBO signals in angular momentum and wave forcing. Geophys. Res. Lett. 21: 2717–2720, 1994.

Beljaars, A. C. M., Brown, A. R., & Wood, N.: A new parameterization of turbulent orographic form drag. Quarterly Journal of the Royal Meteorological Society, 130, 1327–1347. https://doi.org/10.1256/qj.03.73, 2004.

Bowman, K. P.: Global patterns of the quasi-biennial oscillation in total ozone. *J. Atmos. Sci.,* **46,** 3382–3343, 1989.

Brasseur, G., Hauglustaine, D., Walters, S., Rasch, P., Muller, J., Granier, C., & Tie, X: MOZART, a global chemical transport model for ozone and related chemical tracers 1. Model description. Journal of Geophysical Research-Atmospheres, 103(D21), 28,265–28,289. https://doi.org/10.1029/98JD02397, 1998.

Burkholder, J. B., Sander, S. P., Abbatt, J., Barker, J. R., Huie, R. E., Kolb, C. E., et al.: Chemical kinetics and photochemical data for use in atmospheric studies, evaluation no. 18, JPL Publication 15–10, Jet Propulsion Laboratory, Pasadena, CA. Retrieved from http://jpldataeval.jpl.nasa.gov, 2015.

Bushell, A. C., Anstey, J. A., Butchart, N., et al.:Evaluation of the quasi-biennial oscillation in global climate models for the SPARC QBO-initiative. *Quarterly Journal of the Royal Meteorological Society*, *148*(744), 1459-1489, 2020.

Butchart, N., Andrews, M. B., & Jones, C. D.: QBO phase synchronization in CMIP6 historical simulations attributed to ozone forcing. *Geophysical Research Letters*, 50, e2023GL104401. https://doi.org/10.1029/2023GL104401, 2023.

Butchart, N., Anstey, J. A., Hamilton, K., et al.: Overview of experiment design and comparison of models participating in phase 1 of the SPARC Quasi-Biennial Oscillation initiative (QBOi). *Geoscientific Model Development*, *11*(3), 1009-1032, 2018.

Butchart, N., Charlton-Perez, A. J., Cionni, I., et al.: Multimodel climate and variability of the stratosphere, J. Geophys. Res., 116, D05102, https://doi.org/10.1029/2010JD014995, 2011.

Butchart, N., Scaife, A.A., Austin, J., et al.: Quasi-biennial oscillation in ozone in a coupled chemistry-climate model. J. Geophys. Res.: Atmosphere 108 (D15), 4486, 2003.

Butler, A. H., Sjoberg, J. P., Seidel, D. J., Rosenlof, K. H.: A sudden stratospheric warming compendium, Earth System Science Data. 9 (1): 63–76. doi:10.5194/essd-9-63-2017.

Charron, M., and Manzini, E.: Gravity waves from fronts: Parameterization and middle atmosphere response in a general circulation model. *Journal of the Atmospheric Sciences*, 59(5), 923– 941. https://doi.org/10.1175/1520-0469(2002)059<0923:gwffpa>2.0.co;2, 2002.

Chipperfield, M. P., & Gray, L. J. : Two-dimensional model studies of the interannual variability of trace gases in the middle atmosphere. *Journal of Geophysical Research: Atmospheres*, *97*(D5), 5963-5980, 1992.

Chipperfield, M., Bekki, S., Dhomse, S. et al.: Detecting recovery of the stratospheric ozone layer. Nature 549, 211–218, 2017. https://doi.org/10.1038/nature23681

Chipperfield, M. P., Gray, L. J., Kinnersley, J. S., Zawodny, J.: A two-dimensional model study of the QBO signal in SAGE II NO2 and O3. *Geophysical research letters*, *21*(7), 589-592, 1994.

Coy, L., Wargan, K., Molod, A. M., et al.: Structure and dynamics of the quasi-biennial oscillation in MERRA-2, J. Climate, 29, 5339–5354, 2016.

Danabasoglu, G., Lamarque, J.-F., Bacmeister, J. et al.: The Community Earth System Model Version 2 (CESM2). Journal of Advances in Modeling Earth Systems,12, e2019MS001916. https://doi.org/10.1029/2019MS001916, 2020.

Dunkerton, T. J.: The role of gravity waves in the quasi-biennial oscillation, J. Geophys. Res., 102, 26,053-26,076, 1997.

Elsbury, D., Peings, Y., and Magnusdottir, G.:, Variation in the Holton-Tan effect by longitude, Q. J. Roy. Meteor. Soc., 147,1767–1787, https://doi.org/10.1002/qj.3993, 2021.

Emmons, L. K., Schwantes, R. H., Orlando, J. J., et al.: The Chemistry Mechanism in the Community Earth System Model version 2 (CESM2). Journal of Advances in Modeling Earth Systems, 12, e2019MS001882. https://doi.org/10.1029/2019MS001882, 2020.

Emmons, L. K., Hauglustaine, D. A., Müller, J. F., Carroll, M. A., Brasseur, G. P., Brunner, D., et al.: Data composites of airborne observations of tropospheric ozone and its precursors. Journal of Geophysical Research-Atmospheres, 105(D16), 20497–20538. https://doi.org/10.1029/2000jd900232, 2000.

Garfinkel, C. I., Shaw, T. A., Hartmann, D. L., and Waugh, D.W.: Does the Holton-Tan Mechanism Explain How the Quasi-Biennial Oscillation Modulates the Arctic Polar Vortex?, J. Atmos. Sci., 69, 1713–1733, https://doi.org/10.1175/JAS-D-11-0209.1, 2012.

Gettelman, A., & Morrison, H.: Advanced two-moment bulk microphysics for global models. Part I: Off-line tests and comparison with other schemes. Journal of Climate, 28, 1268–1287. https://doi.org/10.1175/JCLI-D-14-00102.1, 2015.

Giorgetta, M. A., Manzini, E., and Roeckner, E.: Forcing of the quasi-biennial oscillation from a broad spectrum of atmospheric waves. *Geophysical Research Letters*, *29*(8), 86-1, 2002.

Golaz, J.-C., Van Roekel, L. P., Zheng, X. et al. : The DOE E3SM Model version 2: Overview of the physical model and initial model evaluation. Journal of Advances in Modeling Earth Systems, 14, e2022MS003156. https://doi.org/10.1029/2022MS003156, 2022.

Golaz, J.-C., Caldwell, P. M., Van Roekel, L. P. et al.: The DOE E3SM coupled model version 1: Overview and evaluation at standard resolution. *Journal of Advances in Modeling Earth Systems*, 11(7), 2089– 2129. https://doi.org/10.1029/2018MS001603, 2019.

Golaz, J.-C., Larson, V. E., & Cotton, W. R. A PDF-based model for boundary layer clouds. Part I: Method and model description. Journal of the Atmospheric Sciences, 59, 3540–3551, 2002.

Gray, L. J., & Dunkerton, T. J.: The role of the seasonal cycle in the quasi-biennial oscillation of ozone. *Journal of Atmospheric Sciences*, *47*(20), 2429-2452, 1990.

Hamilton, K., & Hsieh, W. W.: Representation of the quasi-biennial oscillation in the tropical stratospheric wind by nonlinear principal component analysis. *Journal of Geophysical Research: Atmospheres*, *107*(D15), ACL-3, 2002.

Hamilton, K. : Interhemispheric asymmetry and annual synchronization of the ozone quasi-biennial oscillation. *Journal of Atmospheric Sciences*, *46*(7), 1019-1025, 1989.

Hansen, F., Matthes, K., and Gray, L. J.: Sensitivity of stratospheric dynamics and chemistry to QBO nudging width in the chemistryclimate model WACCM, J. Geophys. Res., 118, 10464–10474, https://doi.org/10.1002/jgrd.50812, 2013.

Hasebe, F.: Quasi-biennial oscillations of ozone and diabatic circulation in the equatorial stratosphere, *J. Atmos. Sci.*, 51, 729–745, 1994.

Hersbach H, Bell B, Berrisford P, et al.: The ERA5 global reanalysis, *Q J R Meteorol Soc*. 2020; 146: 1999–2049. https://doi.org/10.1002/qj.3803, 2020,

Hitchcock, P., Butler, A., Charlton-Perez, A., et al.: Stratospheric Nudging And Predictable Surface Impacts (SNAPSI): a protocol for investigating the role of stratospheric polar vortex disturbances in subseasonal to seasonal forecasts. *Geoscientific Model Development*, *15*(13), 5073-5092, 2022.

Hitchman, M. H., and C. B. Leovy: Estimation of the Kelvin wave contribution to the semiannual oscillation, *J. Atmos. Sci.*, 45, 1462, 1988.

Holton, J. R. and Tan, H.-C.: The quasi-biennial oscillation in the Northern Hemisphere lower stratosphere, J. Meteor. Soc. Japan.,60, 140–148, 1982.

Holton, J. R. and Tan, H.-C.: The influence of the equatorial quasi-biennial oscillation on the global circulation at 50 mb, J. Atmos. Sci., 37, 2200–2208, 1980.

Holton, J. R.: Influence of the annual cycle in meridional transport on the quasi-biennial oscillation in total ozone. *Journal of Atmospheric Sciences*, *46*(10), 1434-1439, 1989.

Holton, J. R., and R. S. Lindzen: An updated theory for the quasi-biennial cycle of the tropical stratosphere, *J Atmos. Sci.*, 29, 1076, 1972.

Horowitz, L. W., Walters, S., Mauzerall, D. L., Emmons, L. K., Rasch, P. J., Granier, C., et al.: A global simulation of tropospheric ozone and related tracers: Description and evaluation of MOZART, version 2. Journal of Geophysical Research-Atmospheres, 108(D24), 4784. https://doi.org/10.1029/2002jd002853, 2003.

Hsu, J. and Prather, M. J.: Stratospheric variability and tropospheric ozone, J. Geophys. Res.-Atmos., 114, D06102, https://doi.org/10.1029/2008JD010942, 2009.

Hsu, J., and M. J. Prather: Global long-lived chemical modes excited in a 3-D chemistry transport model: Stratospheric N_2O, NO_y, O_3 and CH_4 chemistry, *Geophys. Res. Lett.*, 37, L07805, doi:10.1029/2009GL042243, 2010.

Hsu, J., M. J. Prather, and O. Wild: Diagnosing the stratosphere-to-troposphere flux of ozone in a chemistry transport model, J. Geophys.Res., 110, D19305, doi:10.1029/2005JD006045, 2005.

Isla et al.: Toward the vertical resolution of the next generation of the Community Atmosphere Model, To be submitted, 2024.

Jones, D. B., Schneider, H. R., & McElroy, M. B.: Effects of the quasi-biennial oscillation on the zonally averaged transport of tracers. *Journal of Geophysical Research: Atmospheres*, *103*(D10), 11235-11249, 1998.

Jucker, M., Reichler, T., & Waugh, D. W.: How frequent are Antarctic sudden stratospheric warmings in present and future climate?. *Geophysical Research Letters*, *48*(11), e2021GL093215, 2021.

Kang, M. J., Chun, H. Y., Son, S. W., et al.: Role of tropical lower stratosphere winds in quasi-biennial oscillation disruptions. *Science Advances*, *8*(27), eabm7229, 2022.

Kinnersley, J. S., and Tung, K. K.: Mechanisms for the extratropical QBO in circulation and ozone. *Journal of the atmospheric sciences*, *56*(12), 1942-1962, 1999.

Kinnison, D. E., Brasseur, G. P., Walters, S., Garcia, R. R., Marsh, D. R., Sassi, F., et al.: Sensitivity of chemical tracers to meteorological parameters in the MOZART-3 chemical transport model. Journal of Geophysical Research-Atmospheres, 112(D20), D20302. https://doi.org/10.1029/2006jd007879, 2007.

Lamarque, J. F., Emmons, L. K., Hess, P. G., Kinnison, D. E., Tilmes, S., Vitt, F., et al.: CAM-chem: Description and evaluation of interactive atmospheric chemistry in the Community Earth System Model. Geoscientific Model Development, 5(2), 369–411. https://doi.org/10.5194/gmd-5-369-2012, 2012.

Larson, V. E. : CLUBB-SILHS: A parameterization of subgrid variability in the atmosphere. arXiv:1711.03675v2 [physics.ao-ph], 2017.

Lawrence, B. N. : A gravity-wave induced quasi-biennial oscillation in a three-dimensional mechanistic model. *Quarterly Journal of the Royal Meteorological Society*, *127*(576), 2005-2021, 2001.

Lee, S., Shelow, D., Thompson, A.M., Miller, S.: QBO and ENSO variability in temperature and ozone from SHADOZ, 1998–2005. J. Geophys. Res.: Atmosphere 115 (D18105), 2010.

Lee, H.-H., Tang, Q., and Prather, M.: E3SM Chemistry Diagnostics Package (ChemDyg) Version 0.1.4, Geosci. Model Dev. Discuss. [preprint], https://doi.org/10.5194/gmd-2023-203, 2024.

Leung, L. R., Bader, D. C., Taylor, M. A., and McCoy, R. B.: An introduction to the E3SM special collection: Goals, science drivers, development, and analysis. *Journal of Advances in Modeling Earth Systems*, 12, e2019MS001821, 2020. https://doi.org/10.1029/2019MS001821

Li, Y., Richter, J. H., Chen, C.-C., & Tang, Q.: A strengthened teleconnection of the quasi-biennial oscillation and tropical easterly jet in the past decades in E3SMv1. *Geophysical Research Letters*, 50, e2023GL104517. https://doi.org/10.1029/2023GL104517, 2023.

Lin, S. J., & Rood, R. B.: An explicit Flux-Form Semi-Lagrangian shallow water model on the sphere. Quarterly Journal of the Royal Meteorological Society, 123, 2477–2498.

Lindzen, R. S., and J. R. Holton (1968), A theory of the quasi-biennial oscillation, *J. Atmos. Sci.*, 25, 1095, 1997.

Logan, J. A., M. J. Prather, S. C. Wofsy, and M. B. Mcelroy: Atmospheric Chemistry - Response to Human Influence. Philos T R Soc A, 290, 187-234, 1978.

Lu, B. W., Pandolfo, L., and Hamilton, K.: Nonlinear representation of the quasi-biennial oscillation. *Journal of the atmospheric sciences*, *66*(7), 1886-1904, 2009.

Marquardt, C., & Naujokat, B.: An update of the equatorial QBO and its variability. *World Meteorological Organization-Publications-WMO TD*, *1*, 87-90, 1997.

Maycock, A. C., Randel, W. J., Steiner, A. K., Karpechko, A. Y., Christy, J., Saunders, R., et al.: Revisiting the mystery of recent stratospheric temperature trends, 2018. *Geophysical Research Letters*, 45, 9919–9933. https://doi.org/10.1029/2018GL078035

McFarlane, N. A.: The effect of orographically excited gravity wave drag on the general circulation of the lower stratosphere and troposphere. *Journal of the Atmospheric Sciences*, 44(14), 1775– 1800. https://doi.org/10.1175/1520-0469(1987)044<1775:teooeg>2.0.co;2, 1987.

McLinden, C. A., Olsen, S. C., Hannegan, B., et al.: Stratospheric ozone in 3-D models: A simple chemistry and the cross-tropopause flux, J. Geophys. Res., 105(D11), 14653–14665, doi:10.1029/2000JD900124, 2000.

Mengel, J. G., H. G. Mayr, K. L. Chan, et al.: Equatorial oscillations in the middle atmosphere generated by small-scale gravity waves, Geophys. Res. Lett., 22, 3027-3030, 1995.

Meraner, K., Rast, S., & Schmidt, H. (2020). How useful is a linear ozone parameterization for global climate modeling? Journal of Advances in Modeling Earth Systems, 12, e2019MS002003. https://doi.org/10.1029/2019MS002003

Morgenstern, O., Hegglin, M. I., Rozanov, E., et al.: Review of the global models used within phase 1 of the Chemistry–Climate Model Initiative (CCMI), Geosci. Model Dev., 10, 639–671, https://doi.org/10.5194/gmd-10-639-2017, 2017.

Naujokat, B.: An update of the observed quasi-biennial oscillation of the stratospheric winds over the tropics. J. Atmos. Sci., 43, 1873-1877, 1986.

Orbe, C., Plummer, D. A., Waugh, D. W., et al.: Description and Evaluation of the specified-dynamics experiment in the Chemistry-Climate Model Initiative , Atmos. Chem. Phys., 20, 3809–3840, https://doi.org/10.5194/acp-20-3809-2020, 2020.

Park, M., and Coauthors: Variability of stratospheric reactive nitrogen and ozone related to the QBO. J. Geophys. Res. Atmos., 122, 10 103–10 118, https://doi.org/10.1002/2017JD027061, 2017.

Pahlavan, H. A., Fu, Q., Wallace, J. M., & Kiladis, G. N.: Revisiting the quasi-biennial oscillation as seen in ERA5. Part I: Description and momentum budget. *Journal of the Atmospheric Sciences*, *78*(3), 673-691, 2021a.

Pahlavan, H. A., Wallace, J. M., Fu, Q., & Kiladis, G. N.: Revisiting the quasi-biennial oscillation as seen in ERA5. Part II: Evaluation of waves and wave forcing. Journal of the Atmospheric Sciences, 78(3), 693-707, 2021b.

Park, M., Randel, W. J., Kinnison, D. E., et al.: Variability of stratospheric reactive nitrogen and ozone related to the QBO. *Journal of Geophysical Research: Atmospheres*, *122*(18), 10-103, 2017.

Pawson,S., K. Labitzke, R. LenschowB, et al.: Climatology of the Northern Hemisphere stratosphere derived from Berlin analysesp, art 1, Monthly means, technicalr eport, Ser.A ,7(3), Freie Univ. Berlin, 1993.

PhotoComp: Chapter 6 - Stratospheric Chemistry SPARC Report No. 5 on the Evaluation of Chemistry-Climate Models 194-202, 2010.

Plumb, R. A., and R. C. Bell: A model of the quasi-biennial oscillation on an equatorial beta-plane, Q. J. R. Meteorol. Soc., 108, 335-352, 1982.

Prather, J. M., Remsberg, E. E.: The Atmospheric Effects of Stratospheric Aircraft: Report of the 1992 Models and Measurements Workshop. (M.J. Prather, E.E. Remsberg, Eds.), Satellite Beach, FL, 144+268+352 pp, 1993.

Politowicz, P. A., & Hitchman, M. H.: Exploring the effects of forcing quasi-biennial oscillations in a two-dimensional model. *Journal of Geophysical Research: Atmospheres*, *102*(D14), 16481-16497, 1997.

Randall, D. A., Tziperman, E., Branson, M. D., Richter, J. H., & Kang, W. :The QBO-MJO connection: A possible role for the SST and ENSO. *Journal of Climate*, 1-36, 2023.

Randel, W. J., & Cobb, J. B.: Coherent variations of monthly mean total ozone and lower stratospheric temperature. *Journal of Geophysical Research: Atmospheres*, *99*(D3), 5433-5447, 1994.

Randel, W. J., Wu, F., Russell, J. M., Roche, A., & Waters, J. W.: Seasonal cycles and QBO variations in stratospheric CH4 and H2O observed in UARS HALOE data. *Journal of the atmospheric sciences*, *55*(2), 163-185, 1998.

Randel, W. J., and F. Wu: Isolation of the ozone QBO in SAGE II data by singular value decomposition. *J. Atmos. Sci.,* **53,** 2546–2559, 1996.

Rasch, P. J., Xie, S., Ma, P.-L., et al.: An overview of the atmospheric component of the Energy Exascale Earth System Model. *Journal of Advances in Modeling Earth Systems*, 11(8), 2377– 2411. https://doi.org/10.1029/2019ms001629, 2019.

Reed, R.: A tentative model of the 26-month oscillation in tropical latitudes. Q. J. R. Meteorol. Soc. 90, 441–466, 1964.

Richter, J. H., Anstey, J. A., Butchart, N., Kawatani, Y., Meehl, G. A., Osprey, S., & Simpson, I. R.: Progress in simulating the quasi-biennial oscillation in CMIP models. *Journal Geophysical Research: Atmospheres*, 125, e2019JD032362. https://doi.org/10.1029/2019JD032362, 2020.

Richter, J. H., Chen, C.-C., Tang, Q., et al.: Improved simulation of the QBO in E3SMv1. *Journal of Advances in Modeling Earth Systems*, 11(11), 3403– 3418. https://doi.org/10.1029/2019MS001763, 2019.

Ruiz, D. J., Prather, M. J., Strahan, S. E., et al.: How atmospheric chemistry and transport drive surface variability of N2O and CFC-11. Journal of Geophysical Research: Atmospheres, 126, e2020JD033979. https://doi.org/10.1029/2020JD033979, (2021).

Ruiz, D. J. and M.J. Prather: From the middle stratosphere to the surface, using nitrous oxide to constrain the stratosphere–troposphere exchange of ozone, Atmos. Chem. Phys., 22, 2079– 2093, doi: 10.5194/acp-22-2079-2022, 2022.

Sander, et al. : Chemical kinetics and photochemical data for use in atmospheric studies, evaluation number 15, in JPL Publication 06-2., Jet Propul. Lab., Pasadena, Calif., 2006.

Scaife, A. A., et al. (2014), Predictability of the quasi-biennial oscillation and its northern winter teleconnection on seasonal to decadal timescales, *Geophys. Res. Lett.*, 41, 1752–1758, doi:10.1002/2013GL059160.

Scholz M. and Vigário R.: Nonlinear PCA: a new hierarchical approach, *Proceedings of the 10th European Symposium on Artificial Neural Networks (ESANN)*, pp. 439-444., 2002.

Schwartz, M., Froidevaux, L., Livesey, N., Read, W., and Fuller, R.: MLS/Aura Level 3 Monthly Binned Ozone (O_3) Mixing Ratio on Assorted Grids V005, Greenbelt, MD, USA, Goddard Earth Sciences Data and Information Services Center (GES DISC) [data set], https://disc.gsfc.nasa.gov/datasets/ML3MBO3_005/summary (last access: 30 May 2024), 2021.

Scinocca, J., & Mcfarlane, N.: The parametrization of drag induced by stratified flow over anisotropic orography. Quarterly Journal of the Royal Meteorological Society, 126, 2353–2394. https://doi.org/10.1256/smsqj.56801, 2000.

Shibata, K.: Simulations of Ozone Feedback Effects on the Equatorial Quasi-Biennial Oscillation with a Chemistry–Climate Model. Climate, (9), 123. https://doi.org/10.3390/cli9080123, 2021.

Shuckburgh, E., Norton, W., Iwi, A., & Haynes, P.: Influence of the quasi-biennial oscillation on isentropic transport and mixing in the tropics and subtropics. *Journal of Geophysical Research: Atmospheres*, *106*(D13), 14327-14337, 2001.

Sofieva, V. F., Szelag, M., Tamminen, J., et al.: Updated merged SAGE-CCI-OMPS+ dataset for the evaluation of ozone trends in the stratosphere, Atmos. Meas. Tech., 16, 1881–1899, https://doi.org/10.5194/amt-16-1881-2023, 2023.

Stone, K.A., Solomon, S., Kinnison, D.E., On the identification of ozone recovery. Geophys. Res. Lett. 45, 5158–5165, 2018.

Tang, Q., Prather, M. J., Hsu, et al.: Evaluation of the interactive stratospheric ozone (O3v2) module in the E3SM version 1 Earth system model, Geosci. Model Dev., 14, 1219–1236, https://doi.org/10.5194/gmd-14-1219-2021, 2021.

Tang, Q., Golaz, J.-C., Van Roekel, L. P.: The fully coupled regionally refined model of E3SM version 2: overview of the atmosphere, land, and river results, Geosci. Model Dev., 16, 3953–3995, https://doi.org/10.5194/gmd-16-3953-2023, 2023.

Tang, Q., P. G. Hess, B. Brown-Steiner, and D. E. Kinnison : Tropospheric ozone decrease due to the Mount Pinatubo eruption: Reduced stratospheric influx, *Geophys. Res. Lett.*, 40, 5553–5558, doi:10.1002/2013GL056563, 2013.

Tian, W., Chipperfield, M.P., Gray, L.J., Zawodny, J.M.: Quasi-biennial oscillation and tracer distributions in a coupled chemistry-climate model. J. Geophys. Res.: Atmosphere 111 (D20), 2006.

Tilmes, S., Lamarque, J. F., Emmons, L. K., Kinnison, D. E., Ma, P. L., Liu, X., et al.: Description and evaluation of tropospheric chemistry and aerosols in the Community Earth System Model (CESM1.2). Geoscientific Model Development, 8(5), 1395–1426. https://doi.org/10.5194/gmd-8-1395-2015, 2015.

Tilmes, S., Lamarque, J. F., Emmons, L. K., Kinnison, D. E., Marsh, D., Garcia, R. R., et al.: Representation of the Community Earth System Model (CESM1) CAM4-chem within the Chemistry-Climate Model Initiative (CCMI). Geoscientific Model Development, 9(5), 1853–1890. https://doi.org/10.5194/gmd-9-1853-2016, 2016.

Tung, K. K., and H. Yang: Global QBO in circulation and ozone. Part I: Reexamination of observational evidence. *J. Atmos. Sci.,***51,** 2699–2707, 1994.

Tweedy, O. V., Kramarova, N. A., Strahan, S. E., et al., (2017), Response of trace gases to the disrupted 2015–2016 quasi-biennial oscillation, Atmos. Chem. Phys., 17, 6813–6823, 2017.

van der A, R. J., Allaart, M. A. F., and Eskes, H. J.: Extended and refined multi sensor reanalysis of total ozone for the period 1970–2012, Atmos. Meas. Tech., 8, 3021–3035, https://doi.org/10.5194/amt-8-3021-2015, 2015.

Wallace, J., Panetta, R., and Estberg, J.: Representation of the equatorial stratospheric quasibiennial oscillation in EOF phase space, J. Atmos. Sci., 50, 1751–1762, https://doi.org/10.1175/1520-0469(1993)050<1751:ROTESQ>2.0.CO;2, 1993.

Wang L., Hardiman, S. C., Bett, P. E. et al.: What chance of a sudden stratospheric warming in the southern hemisphere?. Environmental Research Letters, 15 (10): 104038. doi:10.1088/1748-9326/aba8c1. ISSN 1748-9326, 2020.

Wang, W., Hong, J., Shangguan, M., et al.: Zonally asymmetric influences of the quasi-biennial oscillation on stratospheric ozone. Atmospheric Chemistry and Physics, 22(20), 13695-13711, 2022.

Watson, P. A. G. and Gray, L. J.: How Does the Quasi-Biennial Oscillation Affect the Stratospheric Polar Vortex?, J. Atmos. Sci., 71, 391–409, https://doi.org/10.1175/JAS-D-13-096.1, 2014.

Xie, F., Zhang, J., Li, X., et al.: Independent and joint influences of eastern Pacific El Niño–southern oscillation and quasi biennial oscillation on Northern Hemispheric stratospheric ozone, Int. J. Climatol., 12, 5289–5307, https://doi.org/10.1002/joc.6519, 2020.

895 Xie, S., Lin, W., Rasch, P. J., et al.: Understanding cloud and convective characteristics in
896 version 1 of the E3SM Atmosphere Model. Journal of Advances in Modeling Earth Systems,
897 10(10), 2618– 2644. https://doi.org/10.1029/2018ms001350, 2018.
898 Zhang, J., Xie, F., Ma, Z., et al.: Seasonal Evolution of the Quasibiennial Oscillation Impact on
899 the Northern Hemisphere Polar Vortex in Winter, J. Geophys. Res., 124, 12568–12586,
900 https://doi.org/10.1029/2019JD030966, 2019.
901 Zhang, J., Xie, F., Ma, Z., Zhang, C., et al.: Seasonal Evolution of the Quasibiennial Oscillation
902 Impact on the Northern Hemisphere Polar Vortex in Winter, J. Geophys. Res., 124, 12568–
903 12586, https://doi.org/10.1029/2019JD030966, 2019.
904 Zhang, R., Tian,W., and Wang, T.: Role of the quasi-biennial oscillation in the downward
905 extension of stratospheric northern annular mode anomalies, Clim. Dynam., 55, 595–612, 2019.
906 Zhang, J., Chongyang Z., Kequan Z., et al.: The role of chemical processes in the quasi-
907 biennial oscillation (QBO) signal in stratospheric ozone. Atmospheric Environment 244,
908 117906, 2021.
909

910
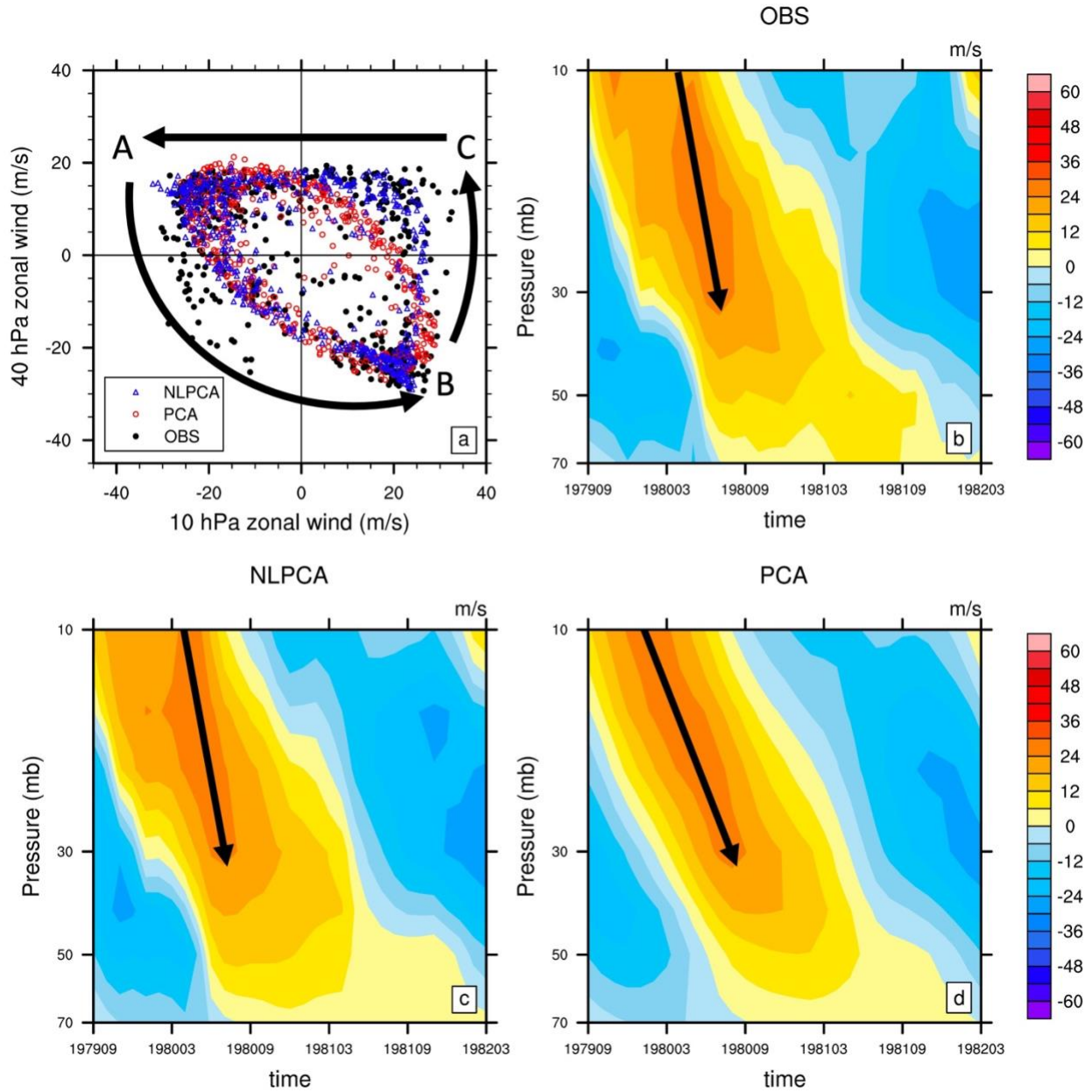
911   Figure 1 (a) Scatter-plot of 1979-2020 monthly mean zonal wind anomaly (m/s) at 10-hPa vs 40-

912   hPa for observation (black), NLPCA reconstruction (blue), and PCA reconstruction (red).

913   Typical cycle of QBO (1979 September-1982 March) from (b) Observational station data from

914   University of Berlin, (c) NLPCA reconstruction, (d) PCA reconstruction.

915

916

917
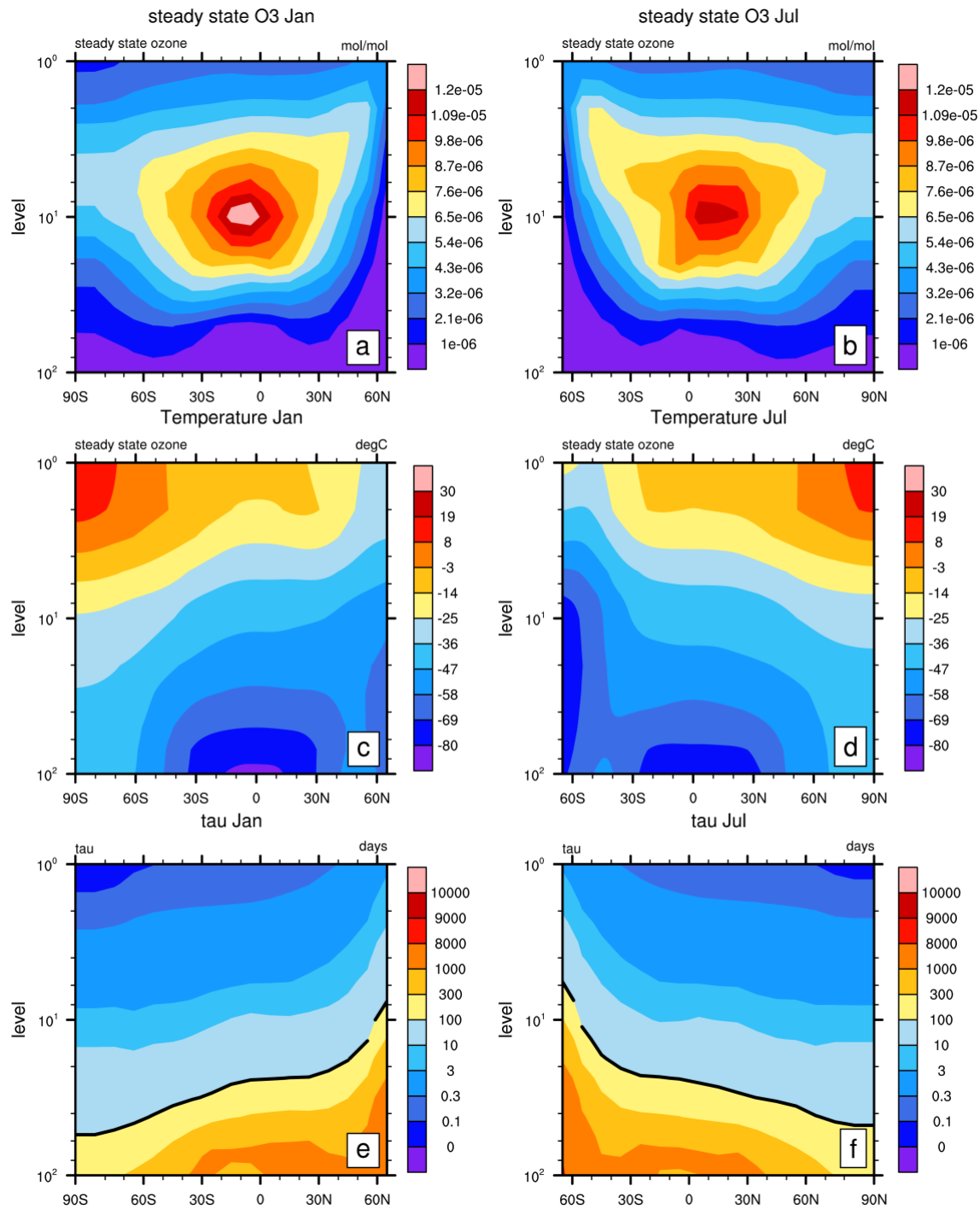
918 Figure 2 The (a, b) steady state ozone (mol/mol) derived using Linoz-v2 on E3SMv2

919 temperature, (c, d) ERA5 temperature (°C), (e, f) photochemical relaxation time τ (days), and for

920 January and July. The thick black line in (c, d) denotes the 300 value-line.

921

922
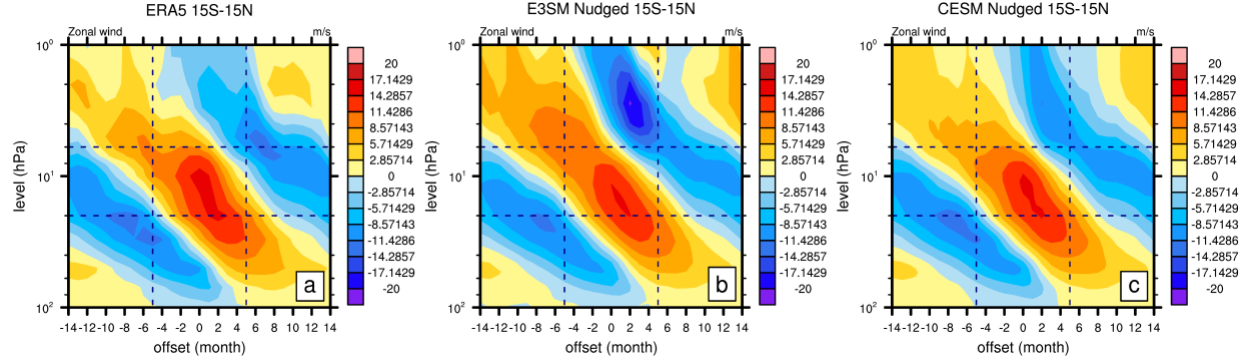
923 Figure 3 Pressure-time cross-section of the tropical (15°S-15°N) zonal wind anomaly (m/s) as

924 function of QBO phase for (a, d) ERA5, (b, e) E3SMv2, (c, f) CESM2 for 1979-2020. 0 is

925 centered on the month when QBO index shifts from QBOe to QBOw (determined by when

926 current QBO index<0 and next QBO index>0). The QBO phase is determined by 5S-5N average

927 of the zonal wind.

928

929

930

931 Figure 4 Pressure-time cross-section of the tropical (15°S-15°N) temperature (K) and $\underline{w}^*$

932 anomaly (Transformed Eulerian Mean residual vertical transport, m/s) as function of QBO phase

933 for (a, d) ERA5, (b, e) E3SMv2, (c, f) CESM2 for 1979-2020. 0 is centered on the month when

934 QBO index shifts from QBOe to QBOw (determined by when current QBO index<0 and next

935 QBO index>0). The QBO phase is determined by 5S-5N average of the zonal wind.

936

937
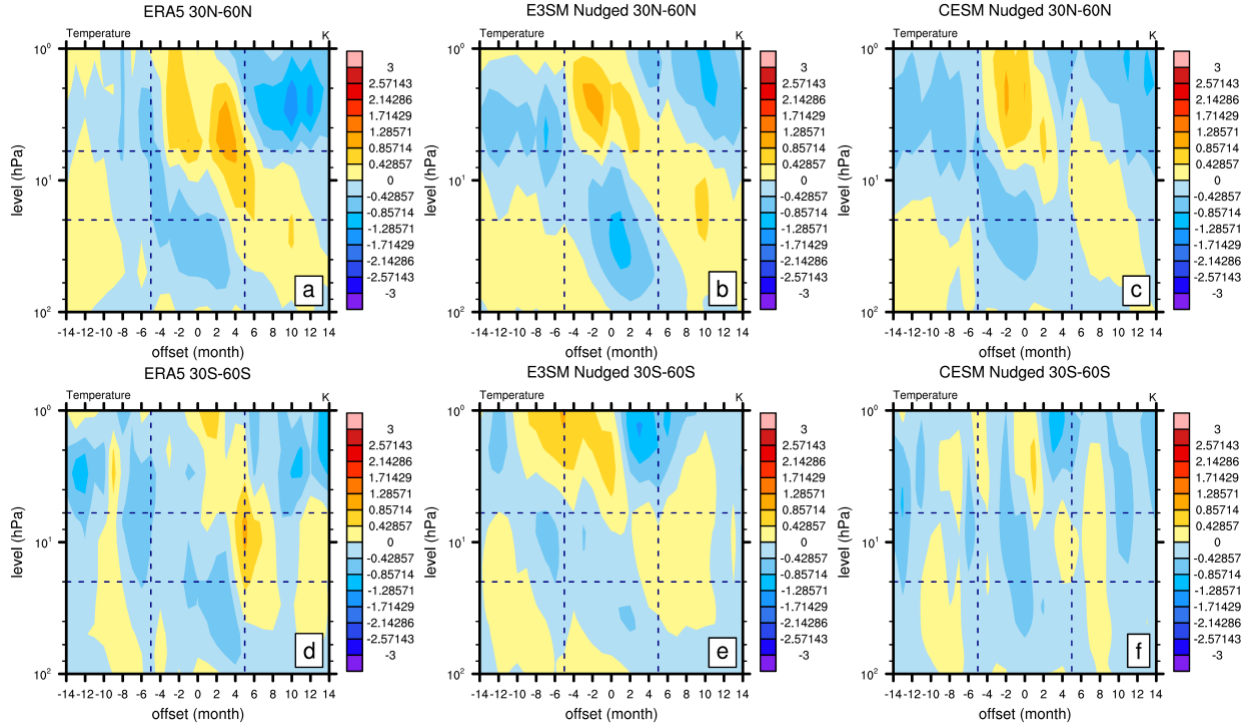
Figure 5 Pressure-time cross-section of the extra-tropical (30°N-60°N/30°S-60°S) temperature

anomaly (K) as function of QBO phase for (a, d) ERA5, (b, e) E3SMv2, (c, f) CESM2 for 1979-

2020. 0 is centered on the month when QBO index shifts from QBOe to QBOw (determined by

when current QBO index<0 and next QBO index>0). The QBO phase is determined by 5S-5N

average of the zonal wind.

943

944

945

946
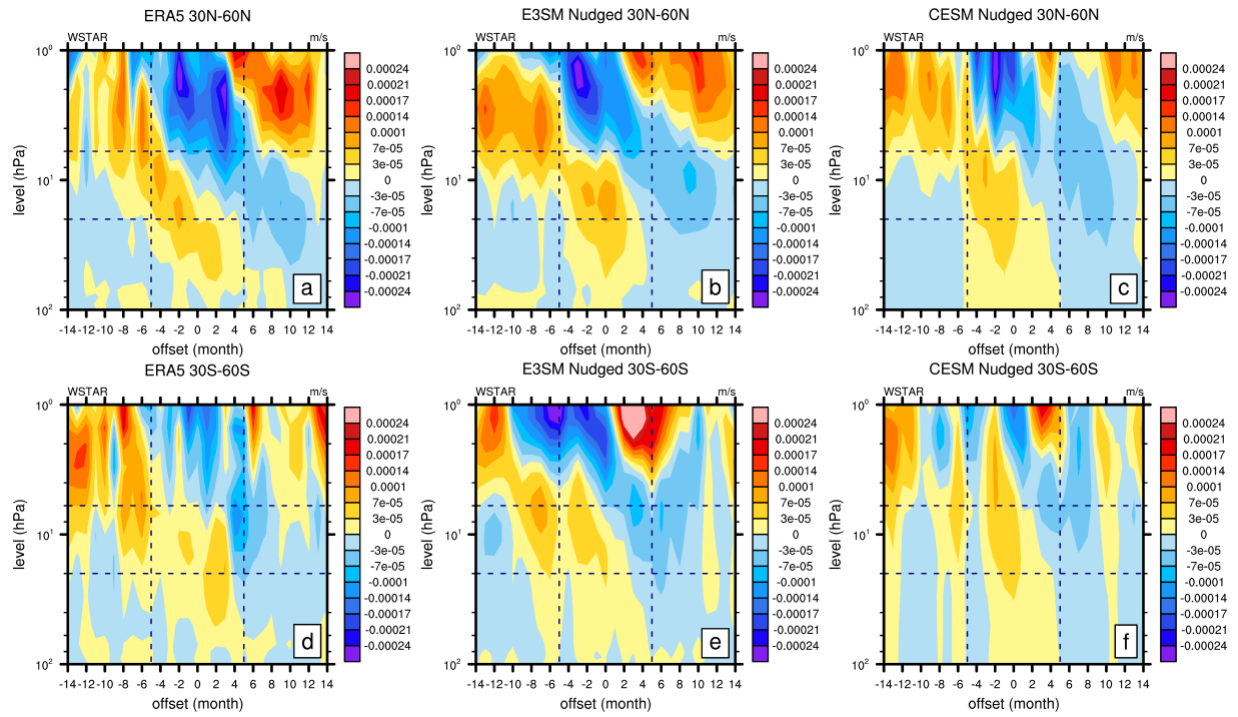
Figure 6 Pressure-time cross-section of the extratropical (30°N-60°N/30°S-60°S) $\underline{w}^*$ anomaly

(m/s) as function of QBO for (a, d) ERA5, (b, e) E3SMv2 nudged, (c, f) CESM2 nudged for

1979-2020. 0 is centered on the month when QBO index shifts from QBOe to QBOw

(determined by when current QBO index<0 and next QBO index>0). The QBO phase is

determined by 5S-5N average of the zonal wind.

952

953

954
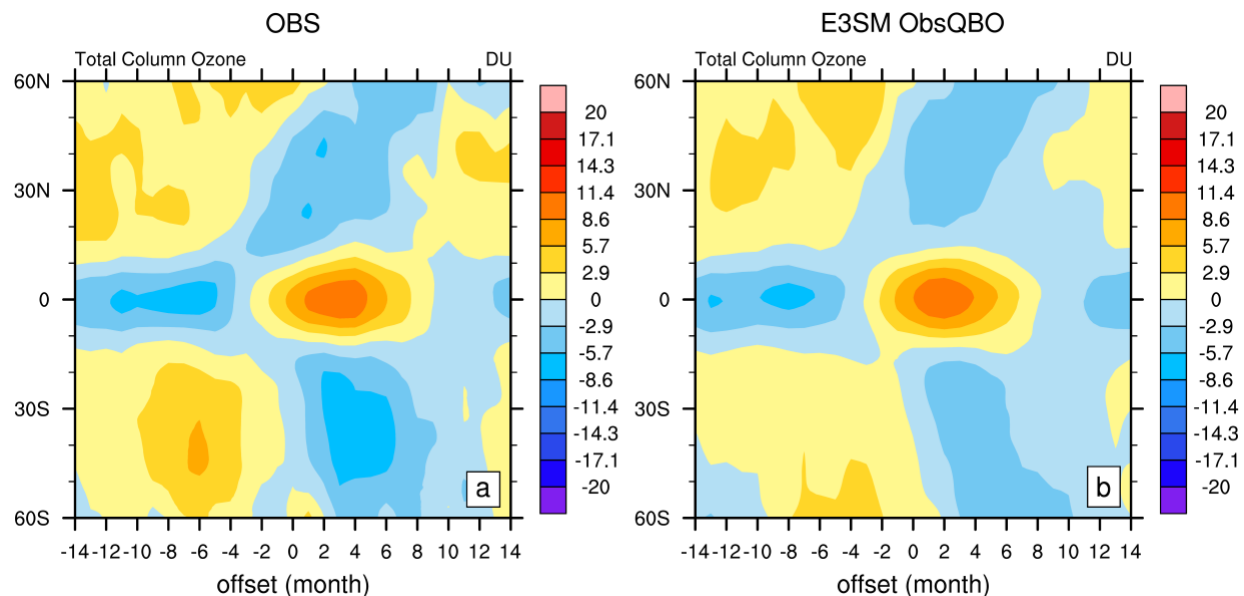
955   Figure 7 Total column ozone (TCO, Dobson Unit) anomaly (relative to 1979-2020 mean)

956   composites as function of QBO phase (determined by NLPCA QBO index) for (a) OBS (Multi-

957   Sensor Reanalysis version 2), (b) E3SMv2 nudged simulation for 1979-2020. 0 is centered on the

958   month when QBO index shifts from QBOe to QBOw (determined by when current QBO

959   index<0 and next QBO index>0). The QBO phase is determined by 5S-5N average of the zonal

960   wind.

961

962
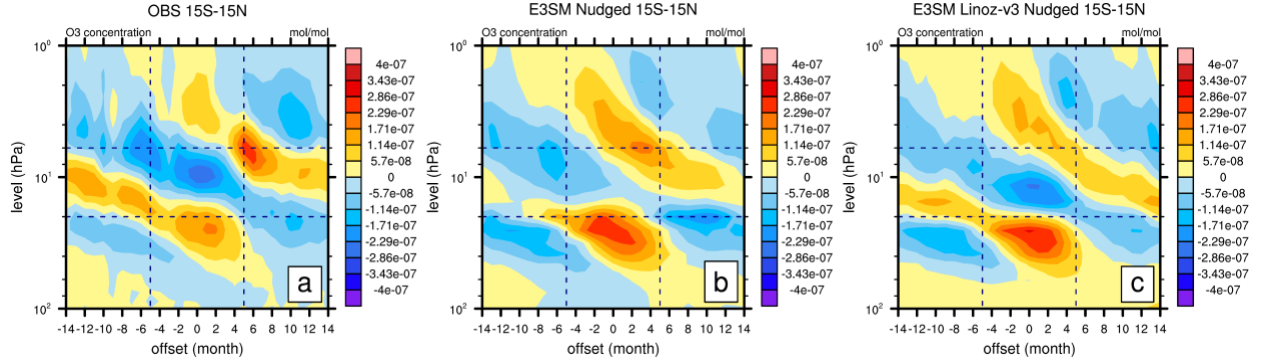
Figure 8 Pressure-time cross-section of the tropical (15°S-15°N) ozone concentration anomaly (mol/mol) as function of QBO phase for (a) Observation (Concentration Monthly Zonal Mean), (b) E3SMv2 nudged simulation, (c) E3SMv2 Linoz-v3 nudged simulation for 1979-2020. 0 is centered on the month when QBO index shifts from QBOe to QBOw (determined by when current QBO index<0 and next QBO index>0). The QBO phase is determined by 5S-5N average of the zonal wind. E3SMv2 Linoz-v3 nudged simulation is produced using nudged E3SMv2 with stratospheric chemistry replaced with Linoz-v3.
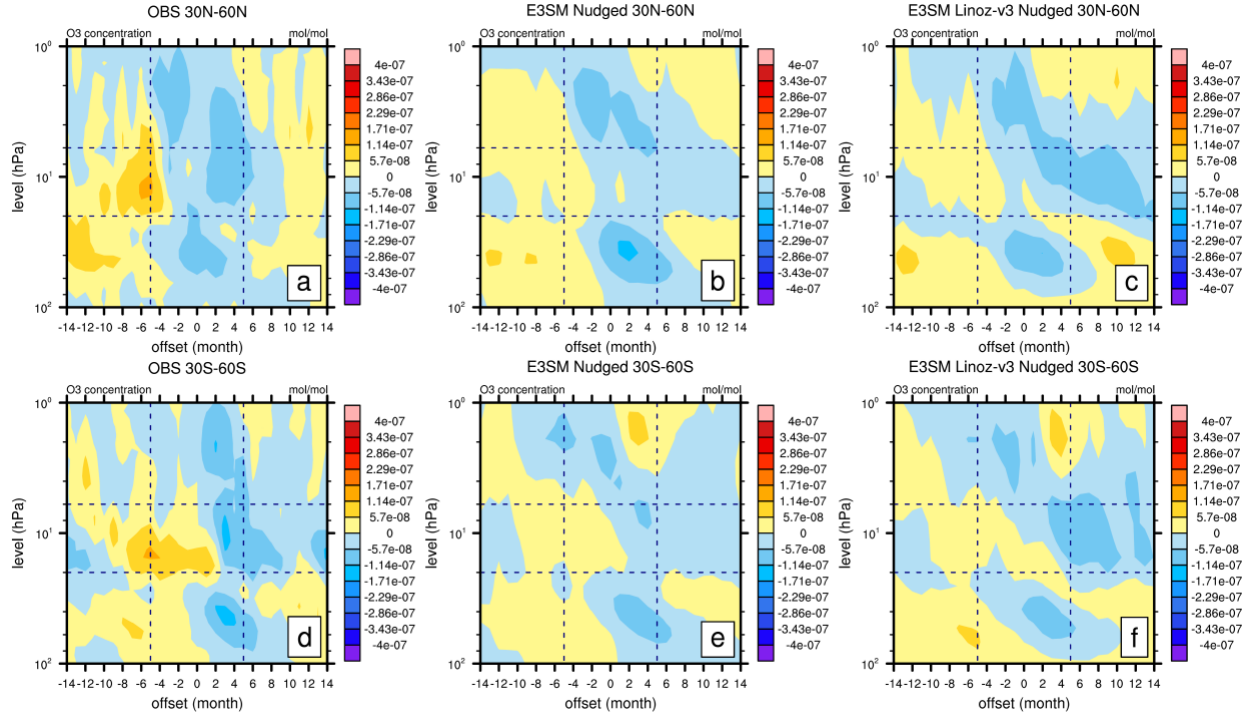
Figure 9 Pressure-time cross-section of the extratropical (30°N-60°N/30°S-60°S) ozone concentration anomaly (mol/mol) as function of QBO phase for (a, d) OBS (CMZM), (b, e) E3SMv2, (c, f) CESM2 for 1979-2020. 0 is centered on the month when QBO index shifts from QBOe to QBOw (determined by when current QBO index<0 and next QBO index>0). The QBO phase is determined by 5S-5N average of the zonal wind. E3SMv2 Linoz-v3 nudged simulation is produced using nudged E3SMv2 with stratospheric chemistry replaced with Linoz-v3.

981
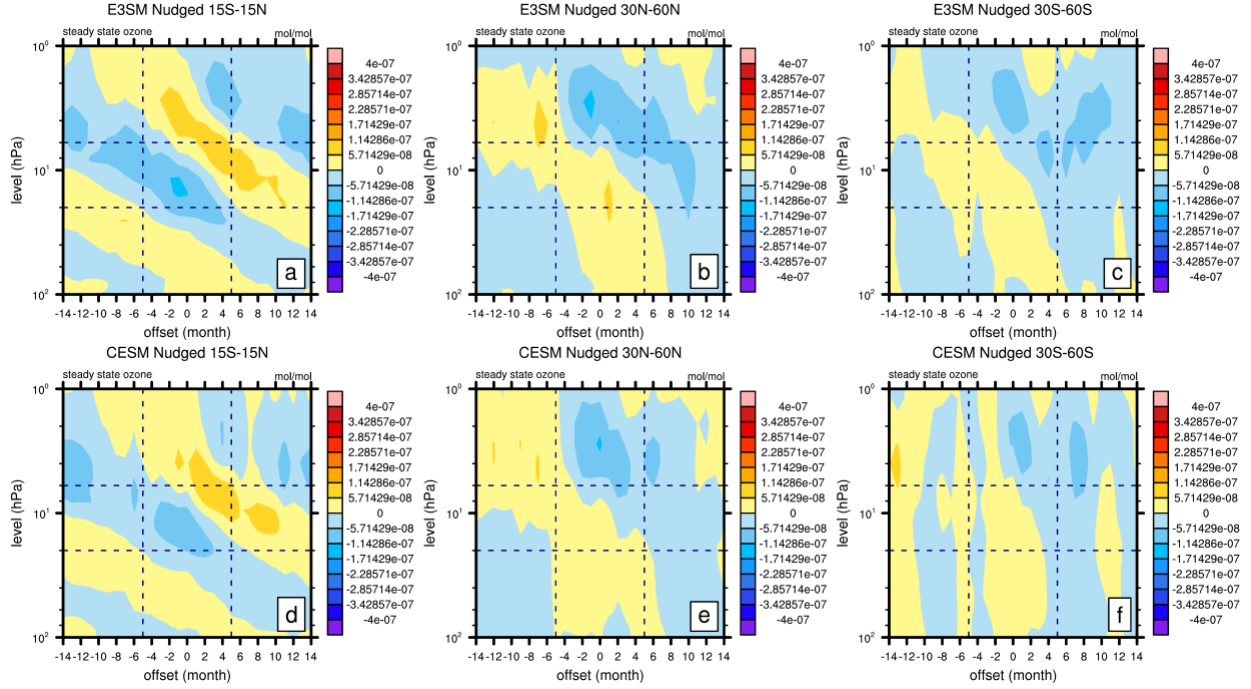
982 Figure 10 Pressure-time cross-section of the tropical (15°S-15°N) and extratropical (30°N-

983 60°N/30°S-60°S) steady state ozone anomaly (mol/mol) as function of QBO phase for (a)

984 E3SMv2 and (b) CESM2 for 1979-2020. 0 is centered on the month when QBO index shifts

985 from QBOe to QBOw (determined by when current QBO index<0 and next QBO index>0). The

986 QBO phase is determined by 5S-5N average of the zonal wind.

987

988
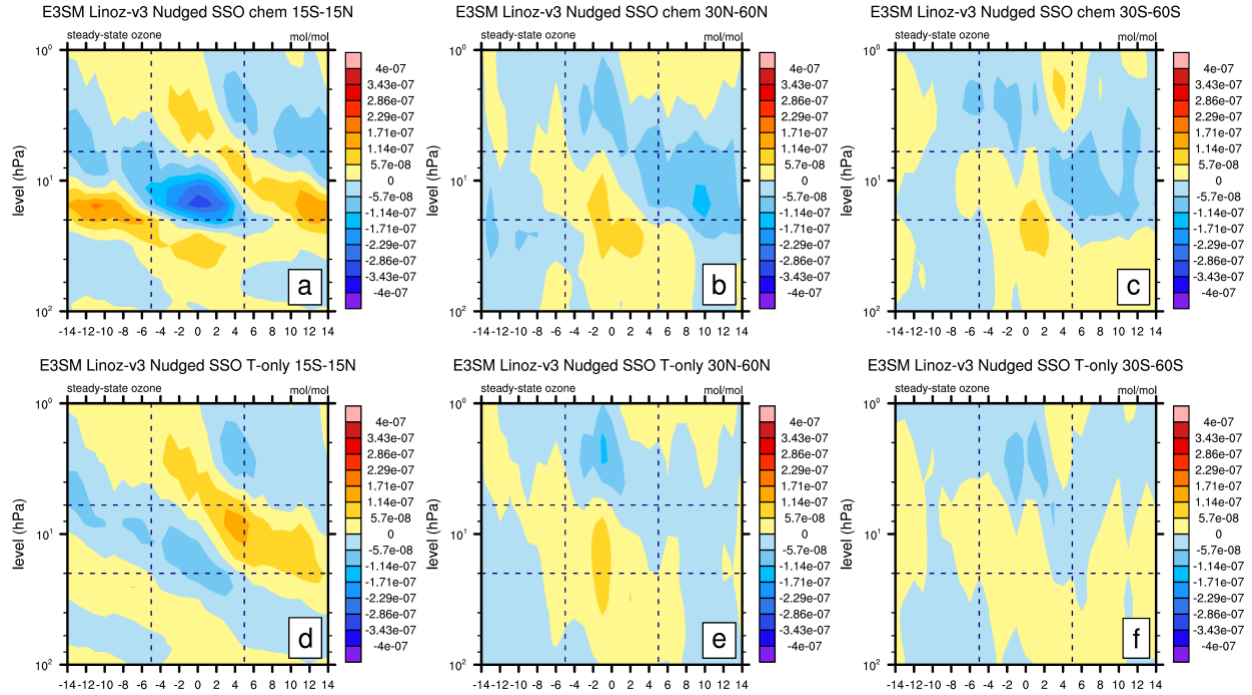
989   Figure 11 Pressure-time cross-section of the tropical (15°S-15°N) and extratropical (30°N-

990   60°N/30°S-60°S) steady state ozone anomaly (mol/mol) as function of QBO for E3SMv2 Linoz-

991   v3 Nudged simulation using (a, b, c) Linoz-v3 chemistry (NO_y-N_2O-CH_4-H_2O), (d, e, f)

992   temperature only for 1979-2020. 0 is centered on the month when QBO index shifts from QBOe

993   to QBOw (determined by when current QBO index<0 and next QBO index>0). The QBO phase

994   is determined by 5S-5N average of the zonal wind.

995

996
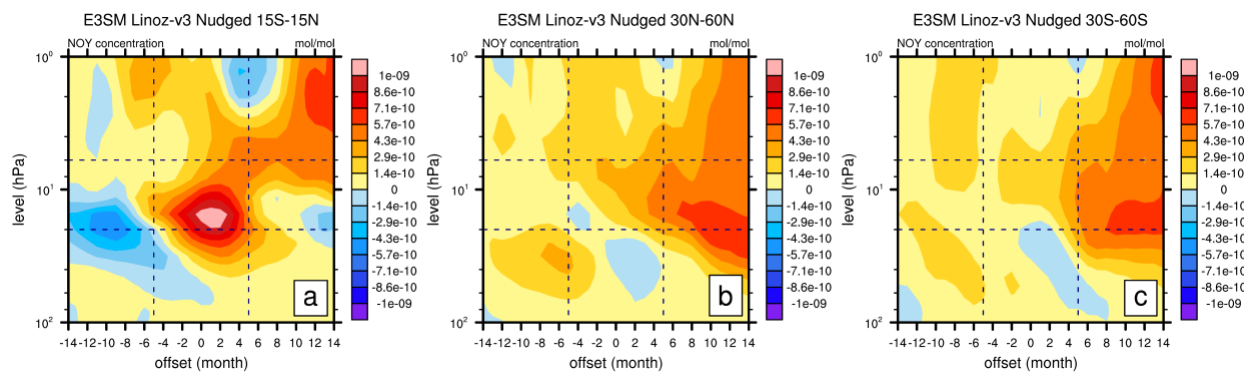
997 Figure 12 Pressure-time cross-section of the tropical (15°S-15°N) and extratropical (30°N-

998 60°N/30°S-60°S) NO$_y$ anomaly (mol/mol) as function of QBO (a, b, c) E3SMv2 Linoz-v3 for

999 1979-2020. 0 is centered on the month when QBO index shifts from QBOe to QBOw

1000 (determined by when current QBO index<0 and next QBO index>0). The QBO phase is

1001 determined by 5S-5N average of the zonal wind.

1002

1003

1004
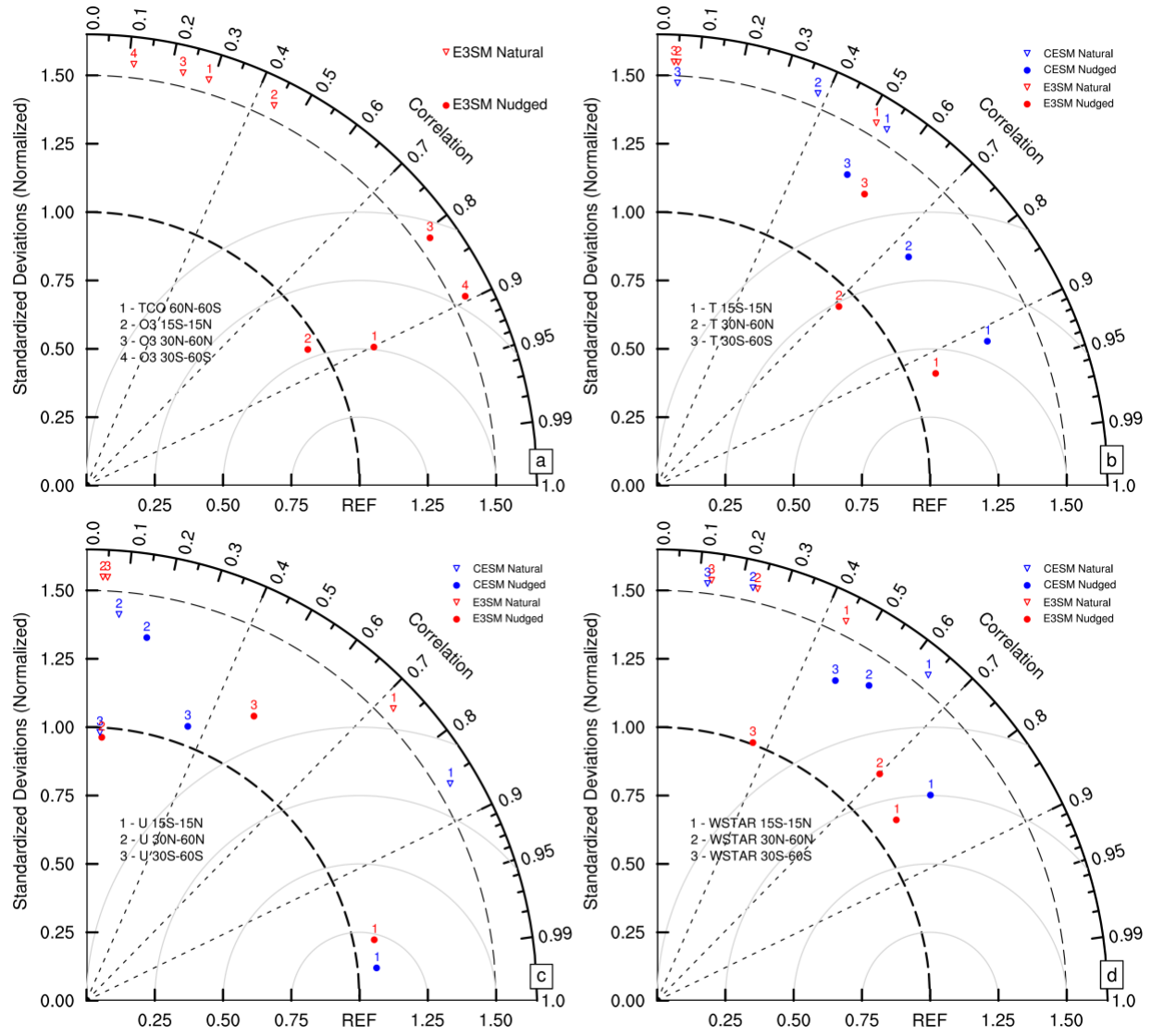
1005 Figure 13 Taylor diagram of the E3SMv2/CESM2 simulation for various datasets for 1979-2020.

1006 (a) The area-weighted total column ozone (60°S-60°N, DU) and pressure-time cross-sections of

1007 ozone concentration (15°S-15°N, 30°N-60°N, 30°S-60°S, mol/mol) anomalies with OBS (MSR

1008 and CMZM), respectively. (b) The area-weighted pressure-time cross-sections of temperature

1009 (15°S-15°N, 30°N-60°N, 30°S-60°S, K) anomalies with ERA5. (c) The area-weighted pressure-

1010 time cross-sections of zonal wind (15°S-15°N, 30°N-60°N, 30°S-60°S, m/s) anomalies with

1011 ERA5. For pattern correlations, the cross-sections are weighted by pressure layer thickness. On

1012 all Taylor diagrams, the model standard deviations are normalized by dividing the standard

1013 deviations of the reference.

1014